International Journal of Engineering Technologies (IJET)

Printed ISSN: 2149-0104
e-ISSN: 2149-5262

Volume:9
No:2
June 2024

Istanbul Gelisim University Press,
2024

CORRESPONDENCE and COMMUNICATION:

Istanbul Gelisim University Faculty of Engineering and Architecture
Cihangir Mah. Şehit P. Onb. Murat Şengöz Sk. No: 8
34315 Avcilar / Istanbul / TÜRKİYE
Phone: +90 212 4227000
Fax: +90 212 4227401
e-Mail: ijet@gelisim.edu.tr
Web site: http://ijet.gelisim.edu.tr
https://dergipark.org.tr/en/pub/ijet
Twitter: @IJETJOURNAL

International Journal of Engineering Technologies (IJET) is included in:

International Journal of Engineering Technologies (IJET) is harvested by the following service:

Organization	URL	Starting Date
The OpenAIRE2020 Project	https://www.openaire.eu	2015
GOOGLE SCHOLAR	https://scholar.google.com.tr/	2015
WORLDCAT	https://www.worldcat.org/	2015
IDEALONLINE	http://www.idealonline.com.tr/	2018
ACADEMINDEX	https://www.academindex.com/journals/31	2022
ACARINDEX	https://www.acarindex.com/journals/international-journal-of-engineering-technologies-3765	2022

INTERNATIONAL JOURNAL OF ENGINEERING TECHNOLOGIES (IJET)
International Peer–Reviewed Journal
Volume 9, No 2, June 2024

Scientific Advisory Board

From the Editor

Dear Colleagues,

On behalf of the editorial board of International Journal of Engineering Technologies (IJET), I would like to share our happiness to publish the 34th issue of IJET. My special thanks are for members of Editorial Board, Publication Board, Editorial Team, Referees, Authors and other technical staff.

Please find the 34th issue of International Journal of Engineering Technologies at http://ijet.gelisim.edu.tr or https://dergipark.org.tr/en/pub/ijet. We invite you to review the Table of Contents by visiting our web site and review articles and items of interest. IJET will continue to publish high level scientific research papers in the field of Engineering Technologies as an international peer-reviewed scientific and academic journal of Istanbul Gelisim University.

Thanks for your continuing interest in our work,

Prof. Dr. Necmettin MARAŞLI
Istanbul Gelisim University
nmarasli@gelisim.edu.tr

----

http://ijet.gelisim.edu.tr
https://dergipark.org.tr/en/pub/ijet
Printed ISSN: 2149-0104
e-ISSN: 2149-5262

International Journal of
Engineering Technologies

IJET

Table of Contents

Volume 9, No 2, June 2024

International Journal of Engineering Technologies, IJET

e-Mail: ijet@gelisim.edu.tr
Web site: http://ijet.gelisim.edu.tr
https://dergipark.org.tr/en/pub/ijet
Twitter: @IJETJOURNAL

Development of a Cassava Grating Machine

Blessing Ngozi Goodluck Aliemeke*‡, Tommy Aisosa Iyore**

* Department of Mechanical Engineering, School of Engineering, Auchi Polytechnic, Nigeria

** Department of Mechanical Engineering, School of Engineering, Auchi Polytechnic, Nigeria

‡Auchi Polytechnic, School of Engineering Auchi, P.M.B. 13 Auchi, Nigeria

(iyoreaisosa@gmail.com, aliemeka@yahoo.com)

‡*Tel: +2348030648051*, *aliemeka@yahoo.com*

Received:24.06.2022 Accepted:03.11.2024

Abstract- Developing of a cassava grating machine is presented. This is a great boost in the development of local content and reduction of wastage in cassava produce in Africa. The use of internal combustion engine in powering the cassava grating machine makes the study unique as it goes a long way in eliminating the undue stress involved manual grating of cassava tubers. The developed machine is made up of components such as hopper, pulley belts, grating unit, internal combustion engine and shaft. Scientific formulae were employed to aid the design of the cassava grating machine. A detailed graphical modeling was done to serve as a guide for the fabrication of the machine. The developed grating machine had a volumetric capacity of hopper to be 50272000 mm^3. A power capacity of 1.715 KW was delivered to the solid shaft of 27.05 mm diameter to grate the peeled cassava tubers at a designed torque of 10.23 Nm.

Keywords: Cassava, Grating, Machine, Design, Internal combustion engine.

1. Introduction

Nigeria is one of the major producers of *Manihotesculenta* specie known as cassava with an average annual input of about 35 million tonnes. Cassava is known to be a tuberous crop of the plant family of *Euphorbiaceae* [1]. Africa is known for its significant progress in agricultural development. To continue standing out among leading nations, there is a crucial necessity to enhance its indigenous resources. The capacity to cultivate crops must be complemented by thorough technological expertise in processing agricultural products. [2].

In the past some researchers in Nigeria developed a manually powered cassava grating machine which had numerous limitations.The development of a cassava grating machine powered by an internal combustion engine for rural African communities embodies several layers of novelty. It addresses local agricultural needs, leverages appropriate technology for non-electrified regions, boosts productivity, and supports socio-economic development. By focusing on mechanical efficiency, portability, local manufacturing, and environmental sustainability, such innovations have the potential to transform rural agriculture, making it more efficient, profitable and sustainable.

In Africa, the cassava is mainly converted to sweet cream white flour known as garri. In a bid to increase this starchy crop production recourse has to be made to the deployment of modern machinery to the cultivating and processing of the crop.

Cassava processing has been in existence for a long time. Africans have been used to the traditional method in which mortar and pestle are applied to the crushing of dried peeled cassava tubers [5]. This method is laborious, time consuming and unhygienic. These deficiencies have led to the development of modern machinery. For a small scale farm the development of cassava processing machine is a welcomed course as a nonexistent of locally made cassava grating machine poses a huge challenge. Before now some researchers have fabricated manually operated cassava grating machine which was considered a bit more useful than the traditional mortar and pestle method. In a bid to bring about improvement in cassava processing an electric motor powered cassava grating machine was designed and constructed by [6].Rural areas often have limited or unreliable access to electricity. Using an internal combustion engine (ICE) as the power source makes the grating machine independent of the electrical grid, ensuring consistent operation even in remote locations. This adaptation is particularly suited to the energy realities of rural African communities [7].

This study is focused on development of cassava grating machine been powered by the internal combustion engine. The machine does not require any electrical power source. It may be used in any rural region without power.

2. Materials and Methods

2.1 Design Considerations

Some design parameters were determined in the course of conceptualizing the development of this machine. The designed parameters are shaft diameter, machine torque, power required, belt speed, length of belt, belt tensions and hopper capacity. In carrying out the parametric design of the grating machine recourse was made to some specifications as obtained from [7] and [8]. The specifications are:

i. Length and breadth of top hopper feature= 400 mm
ii. Length and breadth of bottom hopper feature= 200 mm
iii. Height of hopper=400 mm
iv. Shear stress of mild steel=450 Mpa
v. radius of small pulley=40 mm
vi. radius of large pulley=80 mm
vii. Centre to centre distance of pulleys, a=225 mm
viii. area of leather belt=90 mm^2
ix. length of shaft =350 mm
x. Modulus of rigidity for mild steel =80 GN/m^2
xi. Linear speed, N =1400 m/s
xii. shaft power = 1.5 Kw

2.1.1 Design of Hopper Capacity

The volumetric capacity of the hopper was determined by using equation (1) as obtained from [8].

$$V = \frac{1}{3}[(A_1^2) - (a_1^2)] \times h \qquad (1)$$

where V=volume of hopper

A_1= area of top feature

a_1= area of bottom feature

h = height between the top and bottom feature

$$V = \frac{1}{3}[(400^2) - (200^2)] \times 400 = 50272000\, mm^3$$

The volume of the hopper was calculated to be 50272000 mm^3.

2.1.2 Determination of Length of Belt

The length of open belt was determined by equation (2) obtained from [9].

$$L_b = \pi(R + r) + 2a + \frac{(R - r)^2}{a} \qquad (2)$$

where L_b= length of open belt

R= radius of large pulley

r = radius of small pulley

a = centre to centre distance

The length of belt was determined to be 834.15 mm

Also, the speed of the pulley was determined using equation (3)

$$\frac{N}{n} = \frac{d}{D} \qquad (3)$$

where n =speed of small pulley

d=diameter of small pulley

D=diameter of large pulley

The velocity of belt was determined by the application of equation (4) obtained from [9].

$$v = \omega R \qquad (4)$$

v= velocity of belt

R= radius of large pulley

ω= angular speed

The angular speed of the belt was determined by equation (5) obtained from [10].

$$\omega = \frac{2\pi N}{60} \qquad (5)$$

The angular speed was determined to be 146.63 rad/s for a linear speed of 1400 rpm. Also, the velocity of the belt was calculated to be 11.73 m/s.

2.1.3 Determination of Torque

The torque transmitted by the shaft was determined by equation (6) obtained from [10].

$$T = \frac{60 \times P_s}{2\pi N} \qquad (6)$$

where P_s= Power transmitted by the shaft

T=Torque transmitted

The torque transmitted was determined to be 10.23Nm for a shaft power of 1.5 Kw

The centrifugal force was determined by equation (7) obtained from [10].

$$F = \frac{T}{r} \qquad (7)$$

The centrifugal force was determined to be 255.75 N.

In addition, the stress acting on the leather belt was determined by equation (8).

$$\sigma_b = \frac{F}{A_b} \qquad (8)$$

where σ_b =stress acting on the belt

A_b=area of leather belt

The stress on the belt was determined to be 2.842 N/mm^2.

2.1.4 Determination of Belt Tensions

Also, the maximum tension on the belt was calculated using equation (9) obtained from [11].

$$T = \sigma_b \times t \times b \qquad (9)$$

where T= maximum tension

t= belt thickness

b =belt width

The maximum tension was determined to be 258.622 N from a belt width of 13 mm and thickness of 9 mm

The tension on the tight side was determined by using equation (10).

$$T_1 = T - T_{cf} \qquad (10)$$

where T_1= tension on tight side of the belt in N

T_{cf}=centrifugal tension

Considering centrifugal tension to be negligible, the tension on tight side was determined to be equal to the maximum tension of the belt.

The tension on the slack side of the belt was calculated by the application of equation (11) as given in [11].

$$\frac{T_1}{T_2} = \ell^{\mu\theta} \qquad (11)$$

where T_2=Tension on the slack side in Newton

θ =angle of contact of the smaller pulley in radians.

The angle of contact of the smaller pulley was determined by using equation (12) obtained from [12].

$$\theta = 180 - 2sin^{-1}(\frac{R - r}{a}) \qquad (12)$$

The angle of contact of the smaller pulley was calculated to be 2.7786 radians.

By substitution of angle of contact and a coefficient of friction of 0.3 in equation (11) yielded a slack side tension o f 112.37 N.

2.1.5 Power Transmitted by the Belt

Power transmitted by the belt was determined by applying equation (13) obtained from [12].

$$P = (T_1 - T_2)v \qquad (13)$$

where P= power transmitted in Watt

v=velocity of belt in m/s

$$P = (258.622 - 112.37)11.73 = 1715.54\ W$$

Power transmitted by the belt was calculated to be 1715.54 W by substituting for the belt tensions in equation (13).

2.1.6 Shaft Design

The shaft design was carried out based of rigidity. The polar moment and the shaft diameter of the cassava grating machine were determined by the application of equations (14) and (16) respectively obtained from [12] and [13].

$$\frac{T}{J} = \frac{G\theta_t}{L} \quad (14)$$

where T =Torque in Nm

J=polar moment

G= Modulus of rigidity for mild steel taken to be 80 GN/m^2

θ_t=angle of twist taken to be 0.05^o

L= length of shaft

The polar moment was calculated to be 0.0513 m^4 as shown in equation (15).

$$J = \frac{10.23 \times 0.35}{80 \times 10^9 \times \frac{0.05\times\pi}{180}} = 0.0513\ m^4 \quad (15)$$

The diameter of the shaft was calculated by substituting for the polar moment in equation (16).

$$J = \frac{\pi d^4}{32} \quad (16)$$

where d = diameter of shaft in mm

The shaft diameter was determined to be 27.05 mm.

In addition, the volume and weight of shaft were determined using equations (17) and (18) respectively.

$$V_s = \frac{\pi \times d^2 \times L}{4} \quad (17)$$

Vs=volume of shaft in mm^3

$$V_s = \frac{\pi \times 27.05^2 \times 350}{4} = 201163.3\ mm^3$$

$$W_s = \rho_s \times g \times V_s \quad (18)$$

where Ws= weight of shaft in N

g =acceleration due to gravity taken as 9.81 m/s^2

ρ_s=density of shaft taken to be 7850 kg/m^3

$$W_s = 7850 \times 9.81 \times 0.00020116 = 15.5\ N$$

The machine shaft had a volume and weight of 201163.3 mm^3 and 15.5 N respectively.

2.2 Machine Description

The developed cassava grating machine is comprised of components constructed with steel, including the hopper, internal combustion engine, pulley belt, solid shaft, main frame, and grating unit.

I. Hopper

The hopper shown in Fig. 2 had designed volumetric capacity of 50272000 mm^3. The hopper served as a housing for the peeled and washed cassava tubers as they entered the grating unit.

II. Internal Combustion Engine

The power supply used in the grating machine is by the internal combustion engine designed to have a capacity of 1715.54 Watt. The prime mover utilizes premium motor spirit as fuel.

III. Pulley Belt

The belt and pulley system of power transmission was utilized in this study. The leather belt had dimensions of 13 mm, 9 mm and 834.15 mm for the width, thickness and length respectively. The belt was designed to transmit a power capacity of 1.715 Kw.

IV. Solid Shaft

A solid shaft of 27.05 mm diameter and length of 350 mm was designed on the basis of rigidity to withstand power delivered from the internal combustion engine through pulley belt.

V. Main Frame

The main frame acted as structural support for the grating machine. The frame consists of 50.8 mm angle bar which enhances machine stability and structurally sustained the internal combustion engine, hopper and solid shaft.

VI. Grating Unit

The grating unit consists of perforated sheets, drum and circular discs. The drum is held by shaft and wrapped by perforated rolled cylindrical steel sheet.

3. Results and Discussion

The summary of the designed parameters and detailed graphical modeling are presented in this section.

3.1. Summary of the Designed Parametric Values of the Developed Cassava Grating Machine

The designed values of the Cassava grating machines are shown in Table 1.

Table 1. Summary of designed values of the grating machine

S/N	Machine parameter	Designed value
1	Volume of the hopper	50272000 mm^3
2	Length of belt	834.15 mm
3	Velocity of the belt	11.73 m/s
4	Torque transmitted	10.23 Nm
5	Centrifugal force	255.75 N
6	Stress on the belt	2.842 N/mm^2
7	Maximum tension	258.622 N
8	Power transmitted	1715.54 W
9	Shaft diameter	27.05 mm
10	Volume of shaft	201163.3 mm^3
11	Weight of shaft	15.5 N

The designed parametric values of the cassava grating machine were in agreement with the values of the cassava grating machine designed by [7] and [8].

3.2. Graphical Modelling of the Cassava Grating Machine

The graphical modeling of the developed Cassava grating machine showing the isometric drawing, third angle orthographic projection and the components drawing are shown in Figures 1, 2 and 3 respectively.

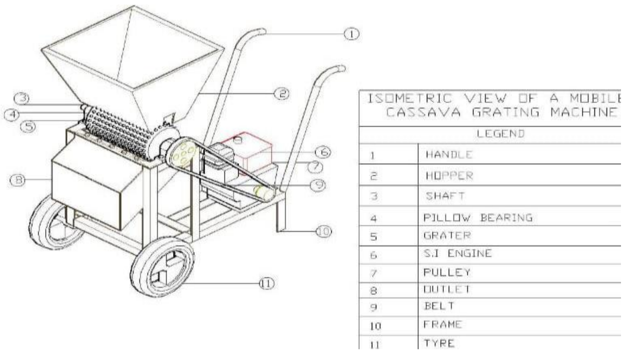

Fig. 1: Isometric drawing of the cassava machine

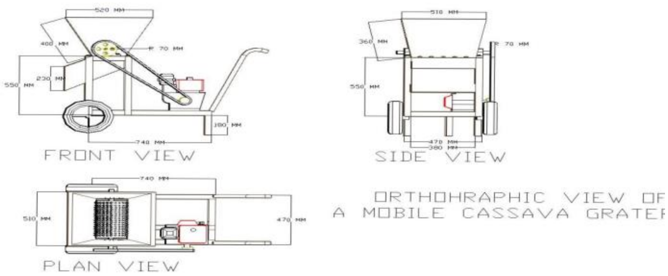

Fig. 2. Third angle orthographic projection of the cassava grating machine

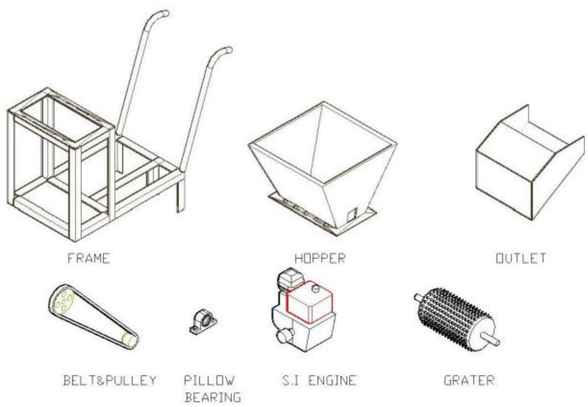

Fig. 3. Components parts of the machine

3.3. Construction of the cassava grating machine

The construction of the machine was carried out using joining processes like welding and riveting. A marking out of components on the main frame of the machine was carried out. The main frame which serves as base and major support for machine components such as hopper, internal combustion engine, grating unit, shaft and pulleys was first constructed using angle bars. Bolts and nuts were used to carry out temporary joining processes for components parts like the internal combustion engine and pulleys. A thorough finishing was done using filing machine in ensuring that every sharp and rough edge was made smooth. In addition, paints were applied to perform the final surface finishing. The developed cassava grating machine is shown in Figure 4.

Fig. 4. Developed cassava grating machine

4. Conclusion

Africa is reputed for its developmental strides in the field of agriculture. In order to remain relevant among the comity of great nations there is a great need to develop its local content. The ability to grow food crops must be matched with the requisite or in depth technological knowhow on processing of agricultural produce. This idea informed the development of cassava grating machine to help convert harvested tubers into various sizes of pellets and powdery form that are served as staple food in many homes across the globe. The cassava grating machine was successfully designed to provide various choices for cassava products. The developed grating machine had a hopper capacity of about 50272000 mm^3 which could contain cassava weight of 20 kg/m^{3}A power capacity of 1715.54 W was delivered to the solid shaft of 27.05 mm diameter to grate the peeled cassava tubers at a calculated torque of 10.23 Nm.

References

[1] O.J. Olukunle and O. M. Jimoh, "Comparative analysis and performance evaluation of Cassava peeling machines", International research Journal of Engineering Science, Technology and Innovation, Vol. 1, No. 4, pp. 94-102, 2012.

[2] E.K. Orhorhoro, A. E. Ikpe and A. N. Ngbeneme, "Analysis of Continuous Cassava Peeling Machine for Domestic and Commercial Use in Nigeria", Journal of the Nigerian Association of Mathematical Physics,Vol. 36, No. 2, pp. 443-448, 2016.

[3] O.R. Adetunji and A.H. Quadri, "Development of a Cassava Grating Machine", Pacific Journal of Science and Technology, Vol. 1, No. 2, pp.120-129, 2016.

[4] B. H. Abdulkadir, "Design and Constructionof a cassava peeling machine", IOSR Journal of Engineering, Vol. 2, No. 6, pp. 1-8, 2012.https://doi.org/10.9790/3021-02630108

[5] E. K. Orhorhoro, P. O. B. Ebunilo and E. G. Sadjere, " Design of Bio-Waste Grinding Machine for Anaerobic Digestive System", European Journal of Advances in Engineering and Technology, Vol.4, No.7, pp. 560-568, 2017.

[6] E. K. Orhorhoro and E. V. Atumah, "Development of a Cassava Peeling Machine", North Asian International Research Journal of Sciences, Engineering and Information Technology, Vol. 3, No. 6, pp. 23-28, 2017.

[7] S.K. Bello, S. B. Lamidi and S. A. Oshinlaja, "Development of Cassava Grating Machine", International Journal of Advances in Scientific Research and Engineering, Vol. 6, No. 10, pp.162-167, 2020.

[8] O. M. Akusu and J. Oluwayomi J., "Development of Dried Cassava Pellets Grinding Machine", American Journal of Engineering Research, Vol. 7, No.3, pp. 46-55, 2018.

[9] B.N.G. Aliemeke, H. A. Okwudibe and O. G. Ehibor, Development of a Fatigue Strength Machine, Nigeria Journal of Technology, Vol. 41, No.2, pp. 256-262, 2022.

[10] R. S. Khurmi and J. K. Gupta, "Theory of Machines", Fourteenth edition, Eurasia publishing Ltd, New Delhi, 2008.

[11] I. S. Oghenevwaire, D. U. Owuamanam and I. S. Anisha, "Development of a Motorized oil palm rotary digester", American Journal of Engineering Research, Vol. 8, No. 12, pp. 195-205, 2019.

[12] R. S. Khurmi and J. K. Gupta, "Machine Design", Revised edition, Eurasia publishing Ltd, New Delhi, 2014.

[13] P. C. Sharma and D. K. Aggarwal, "A Textbook of Machine design", Twelveth edition, S. K. Kataria and sons Publisher, New Delhi, India, 2013.

Numerical Simulations of an Al_2O_3-Water Nanofluid-Based Linear Fresnel Solar Collector

Akpaduado John*, Joseph Oyekale**

* Department of Mechanical Engineering and Mechanics, P.C. Rossin College of Engineering and Applied Sciences, Lehigh University, 27, Memorial Drive West, Bethlehem, PA 18015, USA

* Department of Mechanical Engineering, School of Engineering and Applied Sciences, Federal University of Petroleum Resources Effurun, PMB 1221 Effurun, Nigeria.

Corresponding Author; John Akpaduado; ORCID: 0000-0002-8220-7093, Tel: +1 (835) 240-1884, afj223@lehigh.edu

Second Author: Joseph Oyekale, ORCID: 0000-0003-4018-4660, Tel: +2347033670460, oyekale.oyetola@fupre.edu.ng

Received: 02.08.2022 Accepted: 04.10.2024

Abstract- This study aims to numerically investigate the performance of Al_2O_3-water nanofluid as a heat transfer fluid (HTF) in a linear Fresnel solar receiver. Although a reasonable number of studies have investigated the thermal behaviors of different nanofluids as HTF in solar collectors, the focus has so far been on the parabolic trough collectors, with little or no research efforts available for the linear Fresnel collectors. ANSYS-fluent software was utilized for the simulation in this study, which converted the governing equations to algebraic forms based on the control-volume approach. The Nusselt number and wall temperature were used to characterize the thermal performance of the nanofluid, while the friction factor and eddy viscosity were considered to determine the flow features. The correlation equation proposed by Gnielinski was used to determine the Nusselt number, while the flow features were computed using the Darcy-Weisbach equation. Additionally, the thermal performance of the nanofluid was compared directly with that of pure water. Results showed that the nanofluid improved the thermal performance by about 6-19 % across the solar receiver length. Also, the Nusselt number increases non-uniformly across the length, with a significant rise towards the trailing edge of the nanofluid flow. Conversely, the pressure drop also increases with an increase in the solar receiver length, albeit uniformly. Designers should always factor into the design process to determine the optimum solar collector length when a nanofluid is considered as the HTF; to maximize heat transfer and minimize pressure drop and its attendant economic consequences.

Keywords: Numerical simulation, Nanofluid, Al_2O_3 nanoparticles, Heat transfer analysis, Linear Fresnel collectors, Solar receivers

Nomenclature

Cp	Specific heat, J/kg K
di	Internal diameter of the internal tube, m
do	External diameter of the internal tube, m
f_P	Fiction factor
h	Heat transfer coefficient, W/m2K
k	Thermal conductivity, W/m K
L	Length of tube, m
Nu	Nusselt number
Δp	Pressure drop, Pa
Pr	Prandtl number
v	Fluid velocity, m/s
Al_2O_3	Alumina (aluminum oxide)

Greek letters

ρ	density, kg/m3
μ	dynamic viscosity, kg/ms

1. Introduction

The negative impacts of fossil-fueled energy systems on the environment have necessitated the aggressive focus on clean and renewable energy systems witnessed globally today. Although energy sources such as solar, wind, biomass, hydropower, geothermal, and tidal are mainly on the front burner, other carriers such as hydrogen are also being vigorously explored. In solar energy specifically, several established pathways are available for the exploitation of the thermal energy of the sun, one of which is the Concentrated Solar Power (CSP) route [10]. In CSP systems, collectors are focused on the solar irradiation position by trackers, so that the sun's thermal energy can be accumulated by the heat transfer fluid that flows in the receiver, which is an integral part of the solar collectors. Several practical CSP plants have been built around the world, based on the Parabolic Trough (PT), Linear Fresnel (LF), Solar Tower (Heliostat), and Parabolic Dish technologies [1]. However, solar exploitation is yet to reach a full commercialization stage of development, due to factors such as the transient nature of solar availability, and limitations of heat transfer processes in the solar collectors. Thus, many improvement strategies have been proposed in the literature for decades, and several others are still being proposed to date for the performance enhancement of CSP systems [2–5].

One main strategy for improving the performance of CSP systems that has attracted the attention of energy researchers in recent times is the application of nanofluids for heat transfer enhancement in the collectors [6]. Nanofluids are suspensions of metallic or nonmetallic nanoparticles in a base fluid. They have been explored over the years for use in different sectors of the global economy, but their applications for heat transfer enhancement in renewable energy systems are quite recent [7]. Specifically for the thermal performance improvement of solar collectors which is in focus in this paper, several recent studies are available in the literature, a few of which are critically reviewed in this section. Ashour et al. [4] investigated numerically the thermal performance of ZnO and CuO water nanofluids in a flat-plate solar collector using Egyptian climate conditions. The dedicated 3-D computational fluid dynamics (CFD) model implemented in the study revealed that introducing nanoparticles improved the efficiency of the flat plate solar collector [14-16]. In addition, the study showed that the collector efficiency is influenced by the concentration of the nanoparticles and the heat transfer fluid (HTF) mass flow rate. Similarly, Benabderrahmane et al. [6] analyzed numerically the turbulent forced convection of the dowtherm-A HTF doped with aluminum nanoparticles in a parabolic trough solar receiver. The authors demonstrated that a two-phase model implemented in the study minimizes the need for special correlations to obtain properties of the nanoparticles, relative to a one-phase model. Fahim et al. [8] studied the nanoparticle effects of Cu, Al, and Ti on the thermodynamic performance of thermal oil HTF in parabolic trough solar collectors. They reported that increasing the nanoparticle concentration in thermal oil improved the heat transfer efficiency of the parabolic trough solar collector, with Cu nanoparticles offering the best performance among the three compared. Islam et al. [9] reported similar trends, that a rise in the volumetric concentration of nanoparticles would increase the heat transfer coefficient in parabolic trough solar receivers, based on their joint experimental and numerical study of different nanoparticles. Ying et al.[20] focused on the performance of molten-salt HTF in solar receivers when doped with nanoparticles, and concluded that nanoparticles enhance heat transfer in solar receivers, subject to different concentrations of nanoparticles, inlet velocities of HTF, and heat flux profiles. Abed et al. [1] reported that applications of SiO_2 in Therminol VP-1 as HTF in a parabolic trough solar receiver enhanced performance. However, this enhancement differs in degree for different arrangements of solar inserts into the receiver. Zidan et al. [20] evaluated the performance of 8 different nanoparticles with Therminol VP-1 as HTF in a parabolic trough solar collector hence, reported that TiO_2 yielded the highest enhancement in terms of useful energy, useful exergy, and power block output energy over a year. Additionally, Peng et al. [13] studied the effects of Cu and carbon nanotubes (CNT) on a liquid metal (Gallium) as HTF in a parabolic trough solar receiver. They submitted the addition of nanoparticles enhanced the forced convection heat transfer by about 35-45 %, reduced entropy generation, and increased exergy efficiency; CNT offered a better performance than Cu. However, it was also reported that pressure drop increased in the solar receiver with the introduction of the nanoparticles, relative to what is obtained with pure Gallium. Mahmoudi et al [11] identified CuO-water to offer a better heat transfer enhancement in solar receivers relative to other nanofluids and pure HTF. Mwesigye and Meyer [12] also compared the performance of different nanoparticles in therminol VP-1 as HTF in parabolic trough solar receivers. They highlighted that silver improved the thermal efficiency by about 1.4 percent points over copper, and by about 6.7 percent points over aluminum oxide, with the thermal efficiency increasing with a higher concentration of nanoparticles in therminol VP-1. Babapour et al. [5] experimented with cross-investigating the simultaneous effects of a helically corrugated receiver and nanofluids on the performance of parabolic trough solar collectors. They reported that aluminum nanoparticles increased the Nusselt number by about 220 %, and friction factor by about 146 %, all pointing to the performance enhancement of the parabolic trough receiver. Subramani et al. [17] reported that a further CNT coating of a copper solar receiver with an Al-based nanofluid would improve heat transfer performance. Vahedi et al. [18] however suggested that the improvement of thermal efficiency of thermal oil-based nanofluids in parabolic trough receivers could be negligibly low with increasing Reynolds number. For some nanoparticles that improved performance, the authors reported that they are barely implementable due to the high cost [19].

In the reviewed literature, applications of nanofluids as heat transfer fluids in solar receivers is a viable performance enhancement strategy. Studies reported in the literature review above were focused on the parabolic trough solar technology. Considering that the performance enhancement of solar receivers is case-specific, as seen from the literature review above, it is necessary to investigate the performance of nanofluids as HTF in other solar technologies. The finding aims to numerically study the performance of a linear Fresnel solar receiver using Al_2O_3-water nanofluid as the heat transfer fluid. To the best of the author's knowledge, the study of Al-based nanofluids as HTF in linear Fresnel collectors remains open in the literature, and this constitutes a valid research gap aimed to be filled in this paper. The specific objectives of the study are:

(i) To quantify the thermal effect of Al_2O_3 in water as heat transfer fluid in a linear Fresnel solar receiver;
(ii) To investigate the behavior of heat transfer parameters such as the surface Nusselt number, thermal conductivity, and wall temperature along the solar receiver length; and
(iii) To analyze the variation of flow features such as friction factor and eddy viscosity along the receiver length.

The methods adopted for numerical analysis in this study are reported in section 2; the main results obtained are discussed in section 3; while the conclusions are summarized in section 4.

2. Methodology

2.1. Simulation Set-up, Assumptions, and Nanofluid Properties

An ANSYS-Fluent model was employed in this study to investigate numerically the thermal performance of Al_2O_3-water nanofluid as HTF in a linear Fresnel solar receiver. The simulation determined the HTF outlet temperature across the length of the receiver tube, at varying volume concentrations of the nanoparticle in the fluid. The control volume-based approach was selected for converting the governing equations to algebraic expressions to be solved numerically. There were 11,634 nodes for the adiabatic wall domain (solid) of the tube; 59,001 nodes for the fluid domain (cell) and 11,634 also for the heater surface domain (solid). The schematic view of linear fresnel solar collector is shown in figure 1.

Standard empirical values of density, specific heat capacity, thermal conductivity, and dynamic viscosity of Al_2O_3 and water were each summed up hence, the average values were employed to determine the Prandtl number (Pr) and the Reynolds number (Re_{Dh}). The steady flow of the nanofluid was assumed a constant speed of 35 m/s. The Reynolds number at the tube entrance is large enough to analyze the flow as turbulent. Hence, the thermophysical properties of the nanofluid are constant. A no-slip heat transfer condition was also assumed (heat flux equals zero). The fluid properties and input parameters for the boundary conditions adopted in this study are highlighted in Tables 1 and 2, respectively. Although to adopt this methodology, the Gnielinski correlation is valid for tubes over a large Reynolds number, Re_{Dh} and Prandtl number, Pr. Such that, $3000 \leq Re_{Dh} \leq 5 * 10^6$ and $0.5 \leq Pr \leq 2000$. Hence, the velocity of the fluid must be 35 m/s and above. The ratio of Al_2O_3 to H_2O is 1:1. The mean of the specific heat capacity C_P in J/kgm^3, density ϱ in kg/m^3, thermal conductivity K in W/m^{2}K, and the dynamic viscosity μ in kg/m.s are considered for the modeling. This is done by adding the value of each thermodynamic property such as specific heat capacity, density, thermal conductivity, and dynamic viscosity of Al_2O_3 and the corresponding values of H_2O; then dividing by two.

Table 1. Fluid Properties

Properties at 30 ^{0}C.	H_2O	Al_2O_3	Nanofluid
S. heat, C_P (J/kgm^3)	4184	451	237.5
Density, ϱ (kg/m^3)	997.1	3970	2486.99
Thermal Cond. (W/m^{2}K)	0.6145	12.12	6.3672
Dynamic μ. (kg/m.s)	0.7972	0.8892	0.8432

Density: the mass fraction of nanofluids in water returns to be $x_2 = 0.8$ or 80 %, $x_1 = 1 - x_2$, $\rho_1 = 997.1$ kg/m^3, $\rho_2 = 3970$ kg/m^3. Where ρ_1 and ρ_2 are the density of H_2O and Al_2O_3.

$$\rho = \frac{1}{\frac{x_1}{\rho_1} + \frac{x_2}{\rho_2}} \qquad (1)$$

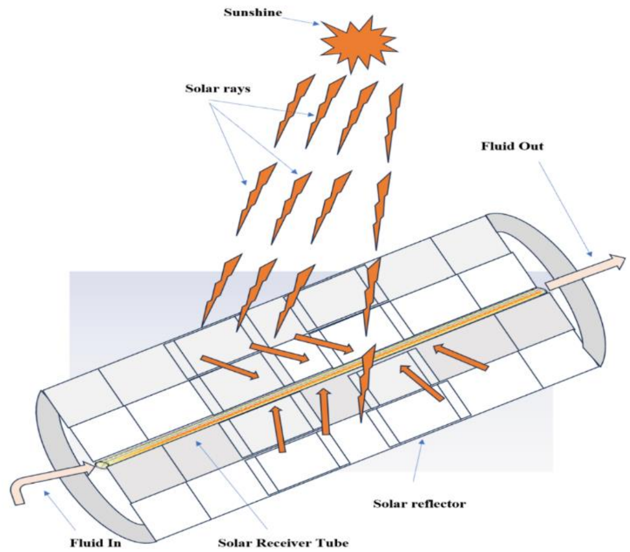

Fig 1. Linear Fresnel solar collector schematic view

Table 2. Input Parameter for Boundary Conditions

Parameter	Value
Pipe outer diameter (m)	0.02
Pipe inner diameter (m)	0.016
Pipe length (m)	1.00
Inlet temperature (^{0}C)	30
Outlet temperature (^{0}C)	30
Inlet velocity (m/s)	63.6
Heat flux (W/m^2)	0 (No-slip condition)
Turbulent intensity	5.063
Pipe material Relative roughness	Steel Commercial Pipe 0.045

Table 3. Steel and Air Properties

Properties at 30 ^{0}C.	Steel	Air
S. heat, C_P (J/kgm^3)	502.416	1.00
Density, 9 (kg/m^3)	8000	1.225
Thermal cond. (W/m^{2}K)	15	0.02225
Dynamic μ. (kg/m.s)	1.793*10^{-3}	1.9*10^{-5}

2.2. Mathematical Correlations

To investigate numerically, the heat transfer performance of Al_2O_3-water nanofluid as HTF in a linear Fresnel solar receiver in this study, the Gnielinski Nusselt number correlation was adopted to predict the thermal profile of the solar receiver. The Gnielinski correlation is valid for tubes over a large Reynolds number range, given by:

$$Nu_{dh} = \frac{(f/8)(Re_{Dh} - 1000)Pr}{1+12.7(f/8)^{1/2}(Pr^{2/3} - 1} \quad (2)$$

f is the Darcy friction factor,

$$(0.790 \ln Re - 1.64)^{-2} \quad (3)$$

Validity of Gnielinski correlation;

$$0.5 \leq Pr \leq 2000$$

$$3000 \leq Re_{Dh} \leq 5 * 10^6$$

Dh is the hydraulic diameter in meters, *Re* is the Reynolds number, *Pr* is the Prandtl number, *Nu* is the Nusselt number, and *f* is the Darcy friction factor. The Darcy–Weisbach model was employed to address the friction factors in the analysis. It is expressed in the head loss form as:

$$\Delta H = (f L v^2 \rho)/2D \quad (4)$$

In pressure loss form:

$$\Delta P = (f L v^2 \rho)/2D \quad (5)$$

where Δh is the head loss due to friction (m), Δp is the pressure loss due to friction (Pa), f_D is the Darcy friction factor, L is the pipe length (m), D is the hydraulic diameter of the pipe (m), ρ is the density (kg/m^2), and v is the mean flow velocity.

Osborne Reynolds proposed; Re, = (density * velocity* diameter) /dynamic viscosity

$$Re = (\rho * v * D) / \mu \quad (6)$$

The velocity of flow was chosen to be 63.6m/s. This assertion was discovered theoretically such that with velocity below this value, the flow will not obey turbulent flow, hence Gnielinski correlation validity.

Re = 3001.1.38

The corresponding Prandtl number Pr = (momentum diffusivity/ thermal diffusivity),

$$Pr = (\mu C_P) / K \quad (7)$$

Pr = 306.90

The Darcy friction factor,

$$f = (0.790 \ln Re - 1.64)^{-2} = 0.0455$$

The Moody diagram called the Stanton diagram (known as the Moody chart) validated the friction factor. This is a graph in a non-dimensional form that relates the Darcy–Weisbach friction factor f_D, Reynolds number Re, and surface roughness for fully developed flow in a circular pipe. It was used to predict pressure drop or flow rate down such a pipe.

Relative toughness = (surface roughness/pipe diameter) = ε /D (8)

Where ε is the relative roughness of the pipe and D is the diameter of the pipe. Blasius (1913) proposed that the friction factor can deduced from the equation,

$$f = 0.3164\ Re^{-0.25} \quad (9)$$

Blasius also proposed that the friction factor depends on Re, for hydraulically smooth pipe and the turbulent flow, the friction factor formula,

$$f = (100.\ Re)^{-0.2} \quad (10)$$

Petuhov concluded in 1970, the friction factor can be achieved from the equation,

$$f = (1.82 \log Re - 1.64)^{-2} \quad (11)$$

where the friction factor is obtained to be 0.0455. Also, according to the Sieder-Tate equation for turbulent flow, although this correlation is largely dependent on Re and Pr,

$$Nu = 0.023\ R_e^{\ 0.8}\ Pr^{\ 1/3}\ [\mu_{\ Al2O3} / \mu_{\ H2O}]^{\ 0.14} \quad (12)$$

Table 3 depicts specific heat capacity values in J/kgm^3, density in kg/m^3, thermal conductivity in W/m^{2}K, and dynamic viscosity in kg/m.s of steel and air at 30 ^{0}C inlet and outlet temperature of Al2O$_3$-water nanofluid in the receiver pipe. Implementing the above equation in ANSYS software made it possible to numerically investigate the thermal energy profile across the length of a linear Fresnel solar receiver when the solar irradiation is focused on it. The Nusselt number and temperatures were used principally to assess the thermal profiles. Also, the flow features were examined across the length of the solar receiver, using the friction factor (pressure loss) and flow viscosity.

3. Results and Discussions

3.1. Mathematical Modeling

The Gnielinski correlation (eqn.1) calculation with a friction factor of 0.0455 depicts that the Nusselt number equals 74.97 and reveals that the Nusselt number increases with an increase in friction factor.

Petukho Nusselt correlation,

$$Nu_{dh} = \frac{(f/8)(Re_{Dh} - 1000)Pr}{1+12.7(f/8)^{1/2}(Pr^{2/3} -1}$$

$Pr > 0.7$, $R_e \leq 2300$

Where: $f = (0.790 \ln R_e - 1.64)^{-2}$ with $R_e = 3001.40$ and f = 0.0455, the correlation justifies that the Nusselt number gives the same value as the corresponding Gnielinski correlation (Nu_{dh}= 75.90). Sieder-Tate equation for turbulent flow, although this correlation is highly dependent on Re and Pr,

$Nu = 0.023\ R_e^{\ 0.8}\ Pr^{\ 1/3}\ [\mu_{\ Al2O3} / \mu_{\ H2O}]^{\ 0.14}$ where μ is the dynamic viscosity for Al_2O_3 and H_2O

The corresponding Nu = 92.45

Table 4 Pipe Variation Concerning Pressure Head

Length (cm)	Pressure loss	Bar
0.2	$25.15 * 10^5$	25
0.4	$50.30 * 10^5$	50
0.6	$75.50 * 10^5$	75
0.8	$100.60 *10^5$	100
1.0	$12.57 * 10^5$	125

Table 4 shows the pressure loss across the length of the solar receiver pipe. The nanofluid obeys the Gnielinski correlation, Pr and corresponding Re_{Dh} of the fluid property are $0.5 \leq Pr \leq 2000$ and $3000 \leq Re_{Dh} \leq 5 * 10^6$. Substituting the fluid thermodynamics properties into the pressure head equation, it is observed that the pressure loss increases across as the pipe increases. Hence, the simulation results from the ANSYS fluent also affirmed this as shown in the pressure drop variation across the solar receiver length in Figure 4.

3.2. Thermal Profile of Al_2O_3-Water Nanofluid Across the Solar Receiver Length

As mentioned earlier, the Gnielinski correlation applied made it possible to predict numerically the heat transfer performance of the linear Fresnel solar receiver using Al_2O_3-water nanofluid as the HTF. Al_2O_3-water nanofluid at 30 ^{0}C flows in the solar receiver pipe with a specific heat capacity of 237.5 J/kgm^3, a density of 2486.99 kg/m^3, the thermal conductivity, and dynamic viscosity of the nanofluid flowing at the velocity of 63.6 m/s are 6.3672 W/m^{2}K and 0.8432kg/m.s respectively. The thermal profile of the HTF across the solar receiver surface is presented in Fig. 2 based on the Nusselt number. As can be seen, there is a non-uniform increase in the Nusselt number along the solar receiver length. While the Nusselt number growth is only moderate for about 95 % of the receiver length from the leading edge, the growth turns significantly high at the trailing edge, becoming almost vertical at the end of the pipe. The significance of this is that there exists a non-uniform thermal profile of the Al_2O_3-water nanofluid across the surface of a solar receiver and that the convective heat transfer tends to increase drastically at the trailing edge of the receiver. When pure water was used as HTF for the simulation, results showed that the Nusselt number (and heat transfer performance) was higher with the use of the applied nanofluid across the length of the receiver, with about 6 – 19 % increase. The ANSYS contours of the entire thermal and flow properties investigated in this study are presented in this paper as an appendix.

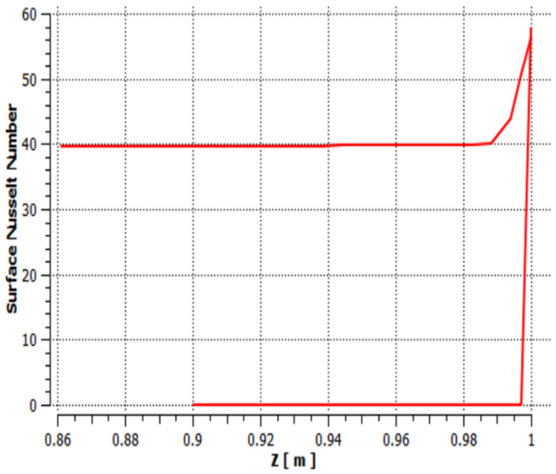

Fig. 2. Surface Nusselt number variation along the solar receiver length

Similarly, the profile of the adjacent wall temperature of the solar receiver is presented in Fig. 3 over the receiver length. As expected, the wall temperature decreases almost linearly from the leading edge to the trailing edge as the nanofluid flows through the solar collector length. This occurs at a constant thermal conductivity of the wall material as shown in Fig. 4. It had been assumed fixed in the simulation set-up.

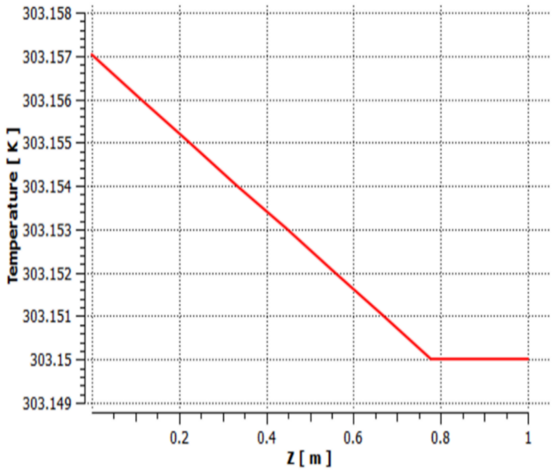

Fig. 3. Wall temperature profile over the length of the solar receiver

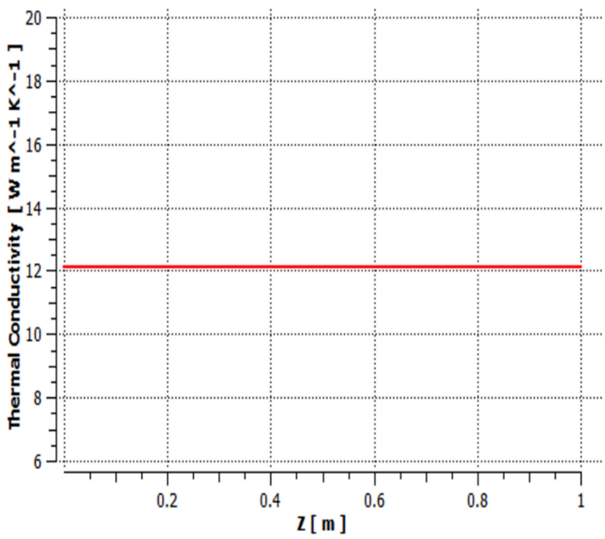

Fig. 4 – Thermal conductivity over the length of the solar receiver

3.3. Flow Features of Al_2O_3-Water Nanofluid Across the Solar Receiver Length

The friction factor measured by pressure drop, and the eddy viscosity, were applied to characterize the flow features of the Al_2O_3-water nanofluid under investigation in this paper for application as HTF in a linear Fresnel solar receiver. Based on the Darcy-Weisbach equation applied in the ANSYS simulation, a trend was obtained for pressure drop variation across the solar receiver length, as shown in Fig. 5. Similarly, the variation of eddy viscosities across the solar receiver length is shown in Fig. 6. As can be seen, increase in solar receiver length also increases the pressure drop, which translates to an increase in friction factor within the flow. This work in contrast relates to the thermal performance illustrated by the Nusselt number in Fig. 2, which increases with an increase in the solar receiver length. These two results imply that due attention must be given to determining the optimum length when applying nanofluid as HTF in a linear Fresnel solar receiver, where the pressure drop would be as low as possible, and the heat transfer coefficient as high as possible. This assertion is corroborated by the result of the eddy viscosity presented in Fig. 6, where the eddy viscosity remains constant over a good distance across the solar receiver, only to ascend drastically towards the trailing edge of the flow. Figure 7 and Figure 8 show the behavior of the Al_2O_3-water nanofluid under the influence of turbulent kinetic energy in square meters per second square ($m^2. s^{-2}$) and the turbulent eddy frequency per second (s^{-1}) across the length of the solar receiver.

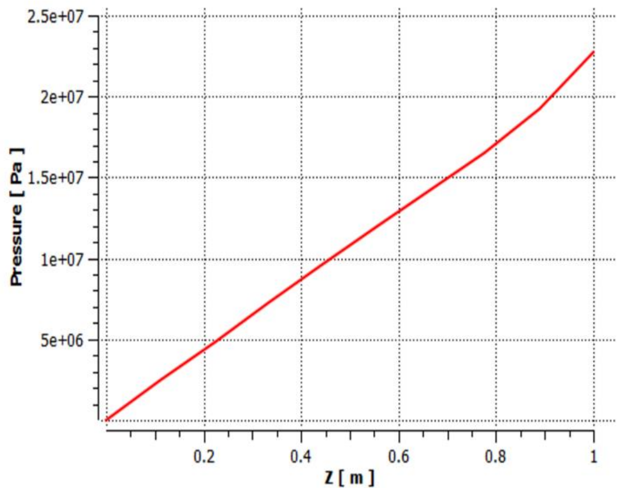

Fig. 5. Pressure drop variation across the solar receiver length

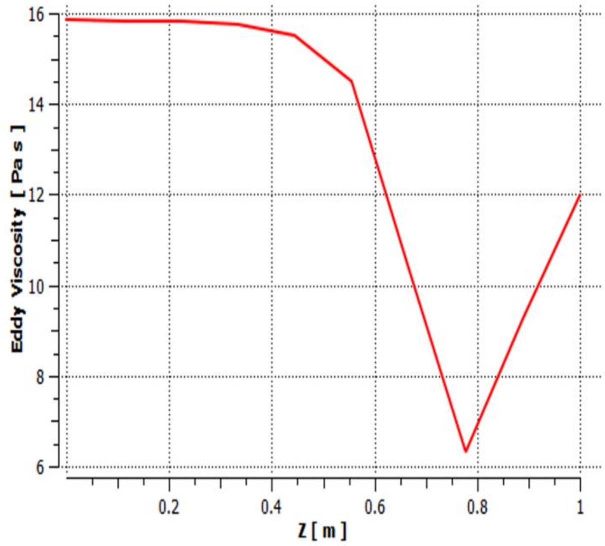

Fig. 6. Effect of receiver length on the eddy viscosity

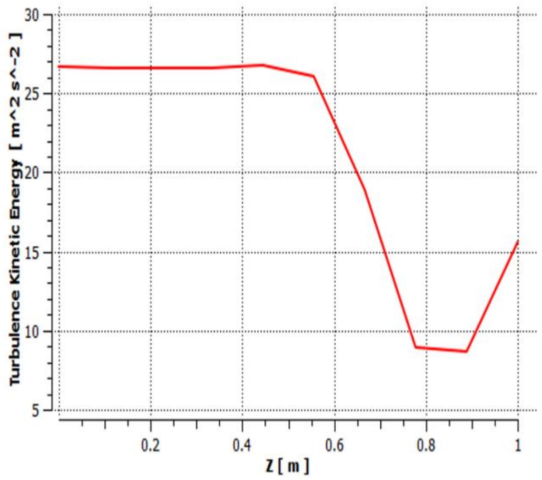

Fig. 7. Turbulent kinetic energy over the length of the solar receiver

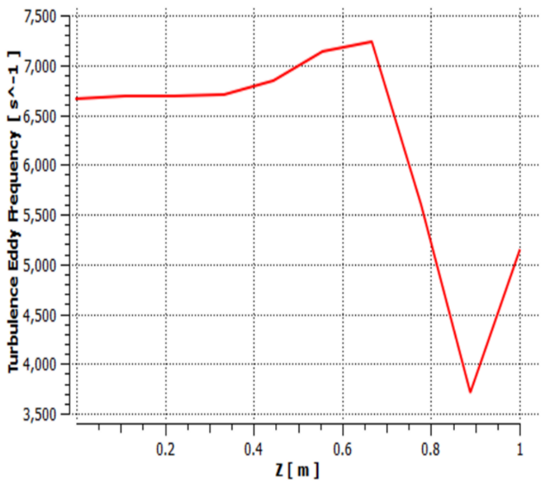

Fig. 8. Turbulent eddy frequency over the length of the solar receiver

Table 5 shows a comparative performance and results of different nanofluids in solar receiver tubes in some reviewed literature. Al_2O_3-water nanofluid as HTF in the solar receiver pipe contours from ANSYS for difference thermal and flow properties which include the pressure, temperature contour, density, velocity, Surface Nusselt Number, surface heat transfer coefficient, skin friction coefficient, thermal conductivity, Al_2O_3-water nanofluid isosurface view, velocity streamline contours, as well as the scale residual of the nanofluid, velocity magnitude against the position in the receiver pipe, and velocity and temperature magnitude contours investigated in the study are shown in Appendix Figure 1 -14 in this paper. Material and absolute roughness property values are also presented in the Appendix Table 1.

Table 5. Comparative nanofluid performance and results with some reviewed works of literature

Reference	Work	Method (s)	Materials	Results
Benabderrahmane et al [6]	Compound heat transfer enhancement numerical analysis using single & two-phase models in PTC receiver	Finite volume method using ANSYS, and K-Ɛ turbulent model.	HTF; nanofluid consisting of Alumina nanoparticles suspended in synthetic oil Dowtherm-A	PTC offers better heat transfer. Darcy friction factor is considerably similar in both single and two-phase modeling
Abed et al [1]	Multiple strips inserts and nanofluids on the thermal-hydraulic performances effect of parabolic trough collectors	Conjugated heat transfers multi-region simple foam (cht Multi Region Simple Foam) engineering tool, Finite-Volume method	Large conical-shaped strips, small conical strips, rectangular-shaped strips, and elliptical-shaped strips. SiO_2 nanoparticles mixed in Therminol® VP-1 (TO)	Nusselt number for large conical strips leads to 57.49 % & 62.53 % for the nanofluid. Thermal conductivity increases to 15.41 %
Carmo Zidan et al [7]	Various nanofluids performance evaluation for parabolic trough collectors	PTC; Parametric Technology Corporation software	Parabolic trough collector, Therminol VP-1, TiO_2	TiO_2 most suitable nanoparticle material to be dispersed in therminol VP-1 for the PTC system.
Ashour et al [4]	Numerical investigation on the thermal performance of a flat plate solar collector	A 3D computational fluid dynamics (CFD) model	water (H_2O), zinc oxide (ZnO) nanofluid, and copper oxide (CuO) nanofluid water-based	H_2O–CuO nanofluid with an average efficiency of about 81.64% at a mass flow rate of 0.0125 kg s^{-1} and VF of 0.15%.
Babapour et al [5]	Helically corrugated receiver and nanofluids PTC; simultaneous effects	ASHRAE standard software (93:2010)	Al_2O_3/water nanofluid at volume fractions of 0.25-1%	An increase of about 219.56% in Nusselt number
This study	Numerical simulations of an Al_2O_3-water nanofluid-based linear Fresnel solar collector	ANSYS Fluent software	Al_2O_3-water nanofluid (Al_2O_3 1:1), linear Fresnel solar collector	Thermal performance increases and the Nusselt number increases by 6-19 % across the pipe length relative to pure water. Friction factors also increase

4. Conclusions

The thermal performance of Al_2O_3-water nanofluid as heat transfer fluid (HTF) in a linear Fresnel solar receiver has been investigated numerically. An ANSYS-Fluent model was adopted to examine the thermal behavior of the nanofluid HTF across the length of the horizontal stainless-steel solar receiver tube. The flow was assumed to be the turbulent flow in the tube with constant properties. The Nusselt number and wall temperature were used principally to investigate the thermal profile of the nanofluid in the solar receiver. Hence the pressure drops and eddy viscosity characterized the flow in the tube. The correlation equation proposed by Gnielinski was used to determine the Nusselt number, while the friction factor was computed using the Darcy-Weisbach equation. The mean of the specific heat capacity C_P in J/kgm^3, density ϱ in kg/m^3, thermal conductivity K in W/m^{2}K, and the dynamic viscosity µ in kg/m.s were considered in the modeling. This is done by adding the value of each thermodynamic property, i.e., specific heat capacity, density, thermal conductivity, and dynamic viscosity of Al_2O_3 and the corresponding values of H_2O; then dividing by two. A direct comparison between the thermal behavior of pure water and the Al_2O_3-water nanofluid showed the potential benefits derived using nanofluid in linear Fresnel solar collector type. The main results obtained from the study are:

- The use of the Al_2O_3-water nanofluid as HTF in a linear Fresnel solar receiver would improve thermal performance (measured by Nusselt number) by about 6-19 % across the length of the receiver, relative to pure water;
- Although the wall temperature decreases almost uniformly along the length of the receiver; the effect of a length on thermal performance is non-uniform, with the highest Nusselt number obtained towards the trailing edge;
- Increasing the length of the receiver resulted in a higher friction factor (measured by pressure drop) for nanofluid flow across the receiver tube.

Lastly, Al_2O_3-water nanofluid as HTF in linear Fresnel should be encouraged due to the potential improvement of the heat transfer performance. Hence, with Al_2O_3-water nanofluid as heat transfer fluid, better efficiency is achievable compared to ordinary water as nanofluid in a solar receiver pipe as proposed in literature. However, the optimum length of the solar receiver that would maximize the heat transfer gain should be determined during design without any extreme increase in the pressure drop and its attendant economic burdens. Contours from ANSYS for the different thermal and flow properties investigated in this study were also presented in the Appendix.

References

[1] Abed, N.; Afgan, I.; Cioncolini, A.; Iacovides, H.; Nasser, A. Effect of various multiple strip inserts and nanofluids on the thermal-hydraulic performances of parabolic trough collectors. *Appl. Therm. Eng.* 2022, *201*, 117798, doi:10.1016/j.applthermaleng.2021.117798.

[2] Ajbar, W.; Parrales, A.; Huicochea, A.; Hernández, J.A. Different ways to improve parabolic trough solar collectors' performance over the last four decades and their applications: A comprehensive review. *Renew. Sustain. Energy Rev.*2022, *156*, doi:10.1016/j.rser.2021.111947.

[3] Al-Oran, O.; Lezsovits, F. Recent experimental enhancement techniques applied in the receiver part of a parabolic trough collector – A review. *Int. Rev. Appl. Sci. Eng.* 2020, *11*, 209–219, doi:10.1556/1848.2020.00055.

[4] Ashour, A.F.; El-Awady, A.T.; Tawfik, M.A. Numerical investigation on the thermal performance of a flat plate solar collector using ZnO & CuO water nanofluids under Egyptian weathering conditions. *Energy* 2022, *240*, doi:10.1016/j.energy.2021.122743.

[5] Babapour, M.; Akbarzadeh, S.; Valipour, M.S. An experimental investigation on the simultaneous effects of a helically corrugated receiver and nanofluids in a parabolic trough collector. *J. Taiwan Inst. Chem. Eng.* 2021, *128*, 261–275, doi:10.1016/j.jtice.2021.07.031.

[6] Benabderrahmane, A.; Benazza, A.; Laouedj, S.; Solano, J.P. Numerical analysis of compound heat transfer enhancement by single and two-phase models in parabolic trough solar receiver. *Mechanika* 2017, *23*, 55–61, doi:10.5755/j01.mech.23.1.14053.

[7] do Carmo Zidan, D.; Brasil Maia, C.; Reza Safaei, M. Performance evaluation of various nanofluids for parabolic trough collectors. *Sustain. Energy Technol. Assessments* 2022, *50*, 101865, doi:10.1016/j.seta.2021.101865.

[8] Fahim, T.; Laouedj, S.; Abderrahmane, A.; Alotaibi, S.; Younis, O. Heat Transfer Enhancement in Parabolic through Solar Receiver : A Three-Dimensional Numerical Investigation. 2022, 1–19.

[9] Islam, M.K.; Hasanuzzaman, M.; Rahim, N.A.; Nahar, A. Effect of nanofluid properties and mass a -flow rate on heat transfer of o parabolic -trough concentrating solar system.

J. Nav. Archit. Mar. Eng. 2019, *16*, 33–44, doi:10.3329/jname.v16i1.30548.

[10] Kumaresan, G.; Sudhakar, P.; Santosh, R.; Velraj, R. Experimental and numerical studies of thermal performance enhancement in the receiver part of solar parabolic trough collectors. *Renew. Sustain. an Energy Rev.* 2017, *77*, 1363–1374, doi:10.1016/j.rser.2017.01.171.

[11] Mahmoudi, A.; Fazli, M.; Morad, M.R.; Gholamalizadeh, E. Thermo-hydraulic performance enhancement of nanofluid-based linear solar receiver tubes with forward perforated ring steps and triangular cross-section; a numerical investigation. *Appl. Therm. Eng.* 2020, *169*, 114909, doi: 10.1016/j.applthermaleng.2020.114909.

[12] Mwesigye, A.; Meyer, J.P. Optimal thermal and thermodynamic performance of a solar parabolic trough receiver with different nanofluids and at different concentration ratios. *Appl. Energy* 2017, *193*, 393–413, doi:10.1016/j.apenergy.2017.02.064.

[13] Peng, H.; Guo, W.; Li, M. Thermal-hydraulic and thermodynamic performances of liquid metal based nanofluid in parabolic trough solar receiver tube. *Energy* 2020, *192*, 116564, doi:10.1016/j.energy.2019.116564.

[14] Răboacă, M.S.; Badea, G.; Enache, A.; Filote, C.; Răsoi, G.; Rata, M.; Lavric, A.; Felseghi, R.-A. Concentrating Solar Power Technologies. *Energies* 2019, *12*, 1048, doi:10.3390/en12061048.

[15] Sandeep, H.M.; Arunachala, U.C. Solar parabolic trough collectors: A review on heat transfer augmentation techniques. *Renew. Sustain. Energy Rev.* 2017, *69*, 1218–1231, doi:10.1016/j.rser.2016.11.242.

[16] Souza, R.R.; Gonçalves, M.; Rodrigues, R.O.; Minas, G.; Miranda, J.M. Recent advances on the thermal properties and applications of nanofluids : From nanomedicine to renewable energies. 2022, *201*, doi: 10.1016/j.applthermaleng.2021.117725.

[17] Subramani, J.; Sevvel, P.; Anbuselvam; Srinivasan, S.A. Influence of a CNT coating on the efficiency of a solar parabolic trough collector using AL2O3 nanofluids - A multiple regression approach. *Mater. Today Proc.* 2021, *45*, 1857–1861, doi:10.1016/j.matpr.2020.09.047.

[18] Vahedi, B.; Golab, E.; Nasiri Sadr, A.; Vafai, K. Thermal, thermodynamic and exergoeconomic investigation of a parabolic trough collector utilizing nanofluids. *Appl. Therm. Eng.* 2022, *206*, 118117, doi: 10.1016/j.applthermaleng.2022.118117.

[19] Wole-osho, I.; Okonkwo, E.C.; Abbasoglu, S.; Kavaz, D. *Nanofluids in Solar Thermal Collectors: Review and Limitations*; Springer US, 2020; Vol. 41; ISBN 0123456789.

[20] Ying, Z.; He, B.; Su, L.; Kuang, Y.; He, D.; Lin, C. Convective heat transfer of molten salt-based nanofluid in a receiver tube with non-uniform heat flux. *Appl. Therm. Eng.* 2020, *181*, doi: 10.1016/j.applthermaleng.2020.115922.

APPENDIX: CONTOURS

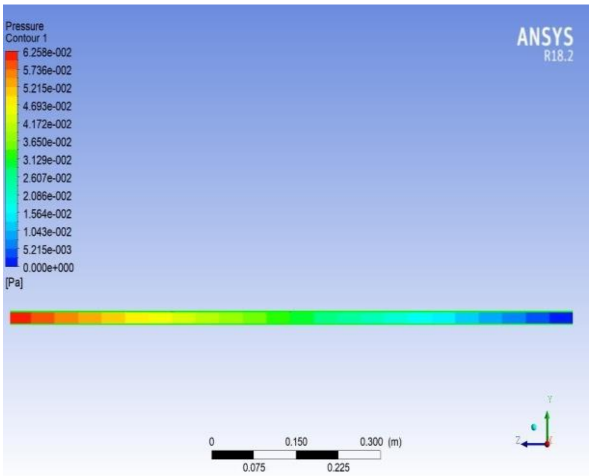

Appendix Fig 1. Pressure contour effect on Al_2O_3-water nanofluid in the Receiver Pipe

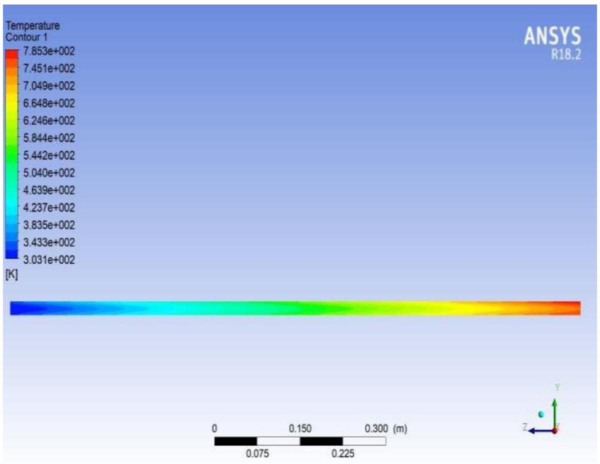

Appendix Fig. 2. Temperature contour on Al_2O_3-water nanofluid in the Receiver Pipe

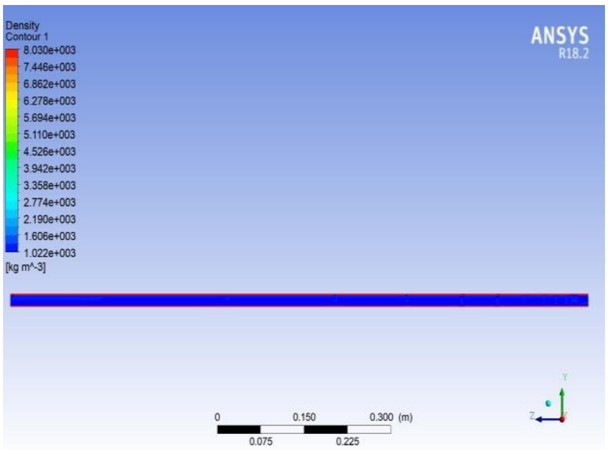

Appendix Fig. 3. Density contour effect on Al_2O_3-water nanofluid in the Receiver Pipe

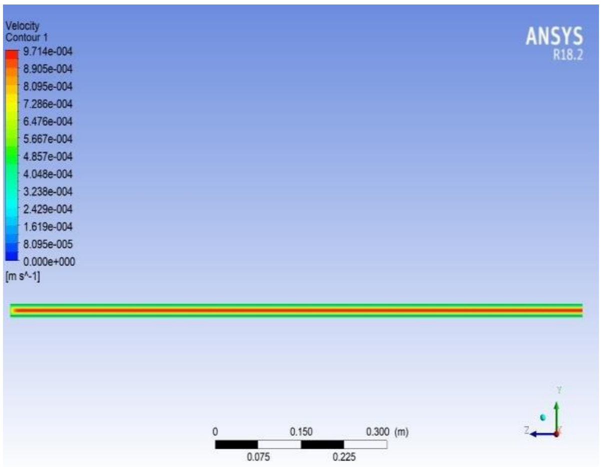

Appendix Fig 4. Velocity contour on Al_2O_3-water nanofluid in the Receiver Pipe

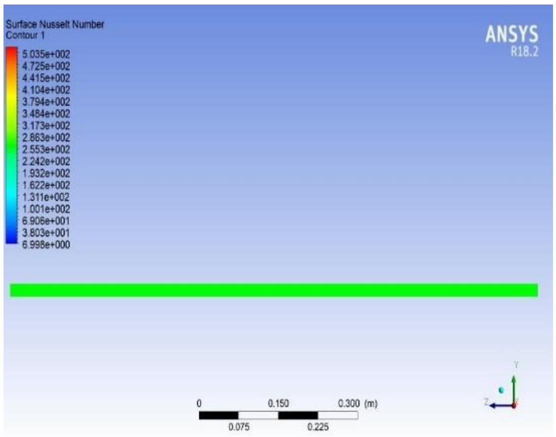

Appendix Fig. 5. Surface Nusselt Number contour on Al_2O_3-water in the Receiver Pipe

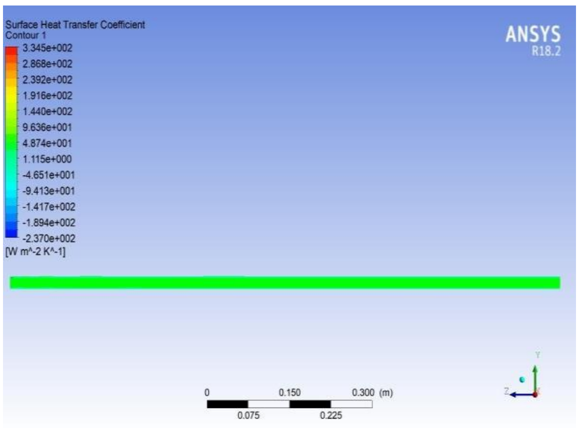

Appendix Fig. 6. Surface Heat transfer coefficient contour on Al_2O_3-water in the Receiver Pipe

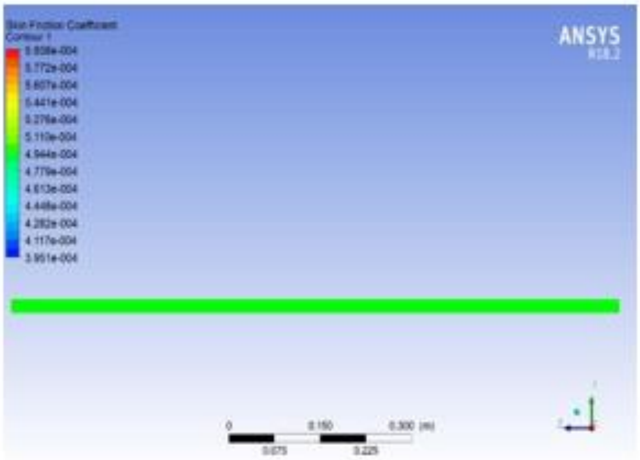

Appendix Fig. 7. Skin Friction Coefficient contour on Al_2O_3-water in the Receiver Pipe

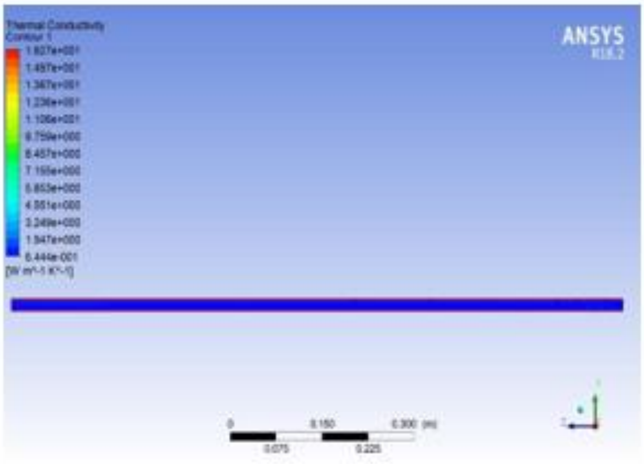

Appendix Fig. 8. Thermal Conductivity Contour on Al_2O_3-water in the Receiver Pipe

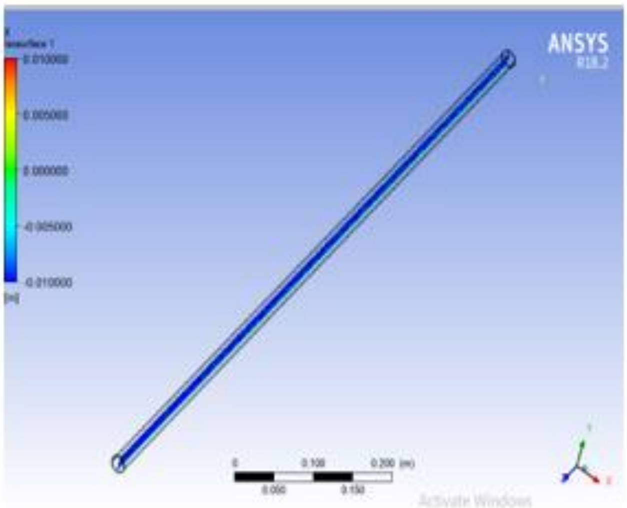

Appendix Fig. 9. Isosurface behavior of Al_2O_3-water in the Receiver Pipe

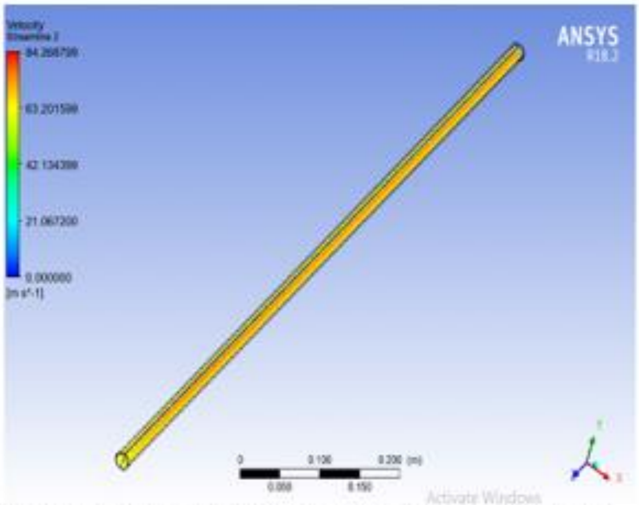

Appendix Fig. 10. Velocity Streamline behavior of Al_2O_3-water in the Receiver Pipe

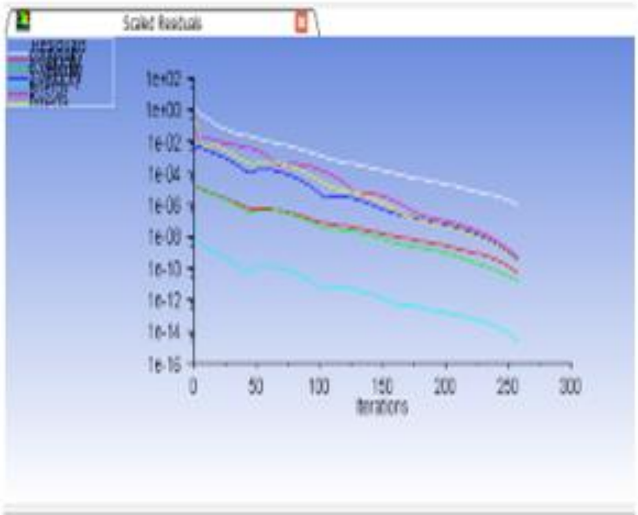

Appendix Fig. 11. Al_2O_3-water nanofluid Scale Residuals in the Receiver Pipe

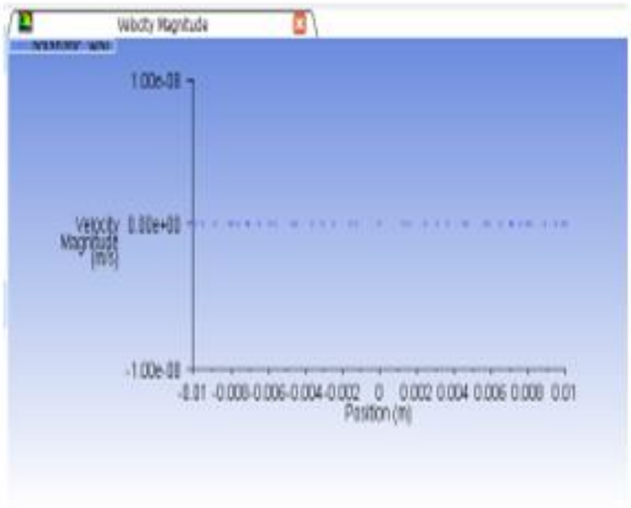

Appendix Fig. 12. Al_2O_3-water nanofluid Velocity Magnitude against Position in the Pipe

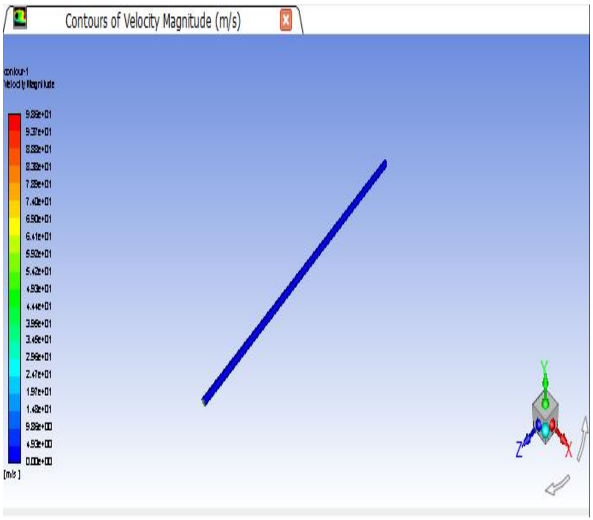

Appendix Fig. 13. Contours of Velocity Magnitude in the Receiver Pipe

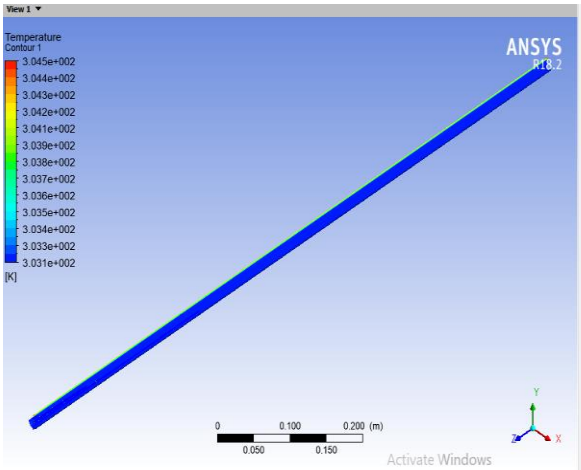

Appendix Fig. 14. Contours of Temperature Magnitude in the Receiver Pipe

Appendix Table 1. Material and Absolute roughness values table

Material	Absolute Roughness (mm)
Copper, Lead, Brass, Aluminum (new)	0.001 - 0.002
PVC and Plastic Pipes	0.0015 - 0.007
Flexible Rubber Tubing - Smooth	0.006-0.07
Stainless Steel	0.0015
Steel Commercial Pipe	0.045 - 0.09
Weld Steel	0.045
Carbon Steel (New)	0.02-0.05
Carbon Steel (Slightly Corroded)	0.05-0.15
Carbon Steel (Moderately Corroded)	0.15-1
Carbon Steel (Badly Corroded)	1-3
Asphalted Cast Iron	0.1-1
New Cast Iron	0.25 - 0.8
Worn Cast Iron	0.8 - 1.5
Rusty Cast Iron	1.5 - 2.5
Galvanized Iron	0.025-0.15
Wood Stave	0.18-0.91
Wood Stave, used	0.25-1
Smoothed Cement	0.3
Ordinary Concrete	0.3 - 1
Concrete – Rough, Form Marks	0.8-3

Mechanical Performance Enhancement of Alkali-Activated Composites Using Synthetic Fibers with Metazeolite and Aluminum Sludge-Based Recycled Concrete Aggregates

Beyza Fahriye Aygün*, Mücteba Uysal**, Ramazan Çingi*

* Department of Civil Engineering, Istanbul University-Cerrahpasa, Üniversite Yolu No:2, 34320 Avcılar, Istanbul, Türkiye.

** Department of Civil Engineering, Yildiz Technical University, Davutpasa 34360, Esenler, Istanbul, Türkiye.

(beyza.aygun@ogr.iuc.edu.tr ; mucteba@yildiz.edu.tr ; ramazancingi@hotmail.com)

Received: 18.05.2024 Accepted: 06.11.2024

Abstract- This study examines the substantial enhancement in the performance of alkali-activated composites (AACs) produced from a distinctive combination of metazeolite (MZ) and slag (S), reinforced with synthetic fibers, and augmented with aluminum sludge (AS) and recycled concrete aggregate (RCA). The composites were subjected to activation through the use of a specific sodium hydroxide (NaOH) and sodium silicate (Na_2SiO_3) blend in a 2:1 ratio, with an activator-to-binder ratio of 0.95. Through a process of experimentation, the research team identified an optimal mix by varying the molarities of sodium hydroxide (NaOH) between 8M and 14M and the ratios of metazeolite to slag between 25% and 100%. The aforementioned mixture, comprising 50% MZ and 50% S, was activated with 12M NaOH and enhanced with 30% aluminum sludge, exhibiting remarkable strength characteristics. Furthermore, the incorporation of synthetic fibres, including polyethylene (PEF), polyamide (PAF), and basalt fibers (BF), resulted in a notable enhancement of the material's performance. It is noteworthy that the addition of basalt fibers at a concentration of 0.5% resulted in a 7% increase in compressive strength and a 24% improvement in flexural strength. This pioneering research illuminates the transformative potential of MZ-S-based AACs, particularly when combined with AS and BF, paving the way for the development of sustainable construction materials that meet contemporary performance and environmental standards.

Keywords: Alkali-activated composites, Metazeolite, Synthetic fibers, Mechanical properties

1. Introduction

In recent years, there has been a notable increase in the advocacy for sustainable development in civil engineering, driven by the growing necessity for eco-friendly and cost-efficient construction materials. The prevailing construction methodologies rely predominantly on Portland cement (PC), which has a considerable environmental impact, accounting for approximately 7% of global CO_2 emissions. In light of the industry's pursuit of more sustainable alternatives, alkali-activated composites (AACs) have emerged as a promising solution, offering a reduction in CO_2 emissions and lower energy consumption. This study examines the innovative application of metazeolite (MZ) and slag (S) in AACs, which are further enhanced with aluminum sludge (AS) and recycled concrete aggregate (RCA) to create high-performance, sustainable building materials. The phenomenon of urbanization has resulted in a notable increase in construction and demolition activities, which in turn has led to a considerable rise in waste generation. In regions prone to seismic activity such as Turkey, urban transformation projects are anticipated to result in the generation of approximately 2 billion tons of construction waste over the next two decades. This scenario presents a unique opportunity to recycle such waste into valuable construction materials, thereby addressing both environmental and economic concerns. The utilisation of recycled aggregates in AACs serves to alleviate waste disposal issues whilst simultaneously reducing the demand for virgin raw materials, thereby aligning with the overarching objectives of sustainable development. Incorporation of diverse fibers has been demonstrated to markedly enhance the mechanical properties of AACs. The integration of synthetic fibers, such as polyethylene (PEF), polyamide (PAF), and basalt fibers (BF), has shown significant promise. These fibers strengthen the structural integrity of AACs by enhancing tensile and flexural strengths, minimizing crack propagation, and improving overall durability. Sahin et al. [3] examined the effects of different basalt fiber ratios in MK-based AACs with various aggregate types. While the mechanical strengths remained within acceptable limits, AACs containing recycled aggregate exhibited slightly reduced properties. In a study by Sahin et al. [3], the effects of varying basalt fiber ratios in MK-based AACs with different aggregate types were examined. While the mechanical strengths remained within acceptable limits, AACs containing recycled aggregate exhibited slightly reduced properties. The unique chemical structures of natural zeolites render them indispensable in the geopolymerization process of AACs. The calcination of these materials at specific temperatures enhances their reactivity, thereby facilitating the formation of robust and durable composites. Zheng et al. [4] conducted a comparative analysis of the frost resistance of concrete using calcined zeolite, demonstrating that the porosity and pore structure exhibited improved characteristics with increasing curing age. Similarly, Florez et al. [5] investigated the calcination-pre-grinding processes of zeolite, revealing enhanced pozzolanic properties. Nikolov et al. [6] employed calcined natural zeolite and clinoptilolite as AAC precursors, resulting in the attainment of considerable compressive strength through potassium silicate activation. Further studies by Ozen and Alam [7] emphasized the significance of activator ratios in the geopolymerization of zeolite-based AACs. Aygörmez [8] conducted an analysis of the high-temperature effects of MK-S-based AACs reinforced with basalt fiber, demonstrating that these materials remain stable even after exposure to temperatures as high as 750 °C. Integrating aluminum sludge (AS) into AACs offers a novel approach to waste management and material enhancement. AS, a by-product of alumina production, is generally seen as a disposal challenge due to its fine particle size and potential environmental impact. However, its inclusion in AACs can aid in setting and enhancing compressive strength, making it a valuable component in sustainable construction materials. This study provides a comprehensive analysis of the synergistic effects of AS and fiber reinforcement in AACs, focusing on their mechanical properties and durability. The combination of zeolite and fibers results in enhanced compressive strength and abrasion resistance. Investigations into ultra-high-performance AACs (UHPAACs) with PPF and SF have shown improved mechanical properties, especially with PPF in SF samples. Non-destructive testing methods, such as UPV, have been used to evaluate SF-reinforced concrete containing recycled nylon granules and zeolite, demonstrating enhanced properties [9-29]. The use of steel fibers (SF) and basalt fibers (BF) has proven effective in boosting the workability and strength of alkali-activated materials (AAMs) or AACs. The concurrent utilization of SF and BF results in a synergistic enhancement in the hardening process, a reduction in stress concentration, and the limitation of crack formation. While SFs enhance the internal structure and properties of the material, BFs facilitate the formation of a well-defined interfacial region, thereby improving water absorption and porosity. By embedding these fibers into adaptable composite materials, it is possible to achieve peak performance while keeping costs low, thus advancing environmental sustainability. Furthermore, the incorporation of natural fiber reinforcement into traditional composites represents a viable and sustainable approach that is environmentally and economically advantageous. The potential of different fibers to enhance the properties of AAC has been investigated by various researchers. In their study, Choi et al. [30] demonstrated that the incorporation of PEF-PVAF reinforcement in S-based AACs resulted in enhanced tensile capacity and healing performance compared to PEF alone. In a related study, Wang et al. investigated the effects of PVAF and nano-silica on MK-S-based AACs, observing significant improvements in strength and durability with optimal PVAF and NS mixtures. In a study by Shaikh [31], PPF was investigated as a reinforcement fiber. The findings indicated that PPF composites exhibited superior mechanical properties with an optimal fiber content of 0-1% by volume.

This study elucidates the eco-technological advantages of sustainable AACs in the construction industry. The global construction industry is a significant contributor to environmental pollution and greenhouse gas emissions, primarily due to the extensive usage of PCs and the accumulation of solid waste. Developed countries have implemented regulatory measures with the objective of controlling PC emissions and promoting the recycling of waste concrete. The importance of recycling cannot be overstated, particularly in light of the significant environmental impact of debris resulting from earthquakes and urban transformations. This research underscores the significance of sustainable AAC production, illustrating the ecological advantages.

2. Materials and Methods

In this study, various materials were employed to create the alkali-activated composites (AACs). Slag (S), obtained from the Bolu Cement Industry, was used due to its high specific gravity (SG) of 2.9 and an impressive 98.6% pass rate through a 45-micron sieve. Mec Energy supplied the zeolite, characterized by a specific gravity of 2.17 and a significant surface area of 9660 cm²/g. The zeolite underwent calcination at 900 °C to enhance its reactivity. Aluminum sludge (AS) was procured from Eti Aluminum AS, dried at 105 °C, and milled to a 90 µm particle size. Recycled concrete aggregate (RCA), provided by a local recycling company, featured an SG of 2.05 and was sieved through a 2 mm sieve to obtain fine aggregates. The chemical activators used included NaOH with a purity exceeding 99% and Na_2SiO_3 containing 27.2% SiO_2, 8.2% Na_2O, with a pH range of 11-12.4. Table 1 presents the chemical compositions of these binder materials. AACs were formulated with a sand-to-binder ratio of 2.5 and an activator-to-binder ratio of 0.95. The weight ratio of Na_2SiO_3 to NaOH was maintained at 2:1, in line with both literature guidelines and preliminary laboratory tests. The initial phase involved creating 16 different AAC mixes, categorized into four series based on varying binder compositions: 100% MZ, 75% MZ + 25% S, 50% MZ + 50% S, and 75% S +25% MZ. Each series was tested with four NaOH molarities: 8M, 10M, 12M, and 14M. The mix that demonstrated the highest strength in this phase underwent further testing with the addition of 10%, 20%, and 30% AS to assess its impact on compressive strength, flexural strength (at 7 and 28 days) and water absorption ratios (at 28 days). In (0.5%, 1%, 1.5%, and 2%) was analyzed for their mechanical properties (Table 2). The final phase, based on the optimal mix of MZ-S and AS, the influence of synthetic fibers—basalt fibers (BF), polyethylene fibers (PEF), and polyamide fibers (PAF)—at various percentages.

Table 1. Chemical composition binder materials.

Component	Slag (%)	Metazeolite (MZ) (%)	Red Mud (RM) (%)	RCA (%)
SiO_2	40.55	76.90	16.20	62.56
Al_2O_3	12.83	13.50	22.90	12.52
Fe_2O_3	1.10	1.40	34.50	5.82
TiO_2	0.75	0.10	-	0.75
CaO	35.58	2.00	1.80	12.0
MgO	5.87	1.10	-	1.83
K_2O	0.68	3.50	-	1.30
Na_2O	0.79	0.30	8.70	2.69
LOI	0.03	1.10	-	-
MnO	-	0.10	-	0.12

Table 2. Mixture contents and quantities.

	MZ (g)	AS (g)	S (g)	RCA (g)	Na_2SiO_3 (g)	NaOH (g)	PEF (g)	PAF (g)	BF (g)
100MZ	450	-	-	1125	142.5	285	-	-	-
75MZ+25S	337.5	-	112.5	1125	142.5	285	-	-	-
50MZ+50S (C)	225	-	225	1125	142.5	285	-	-	-
75S+25MZ	112.5	-	337.5	1125	142.5	285	-	-	-
50MZ+50S+10AS	225	112.5	225	1012.5	142.5	285	-	-	-
50MZ+50S+20AS	225	225	225	900	142.5	285	-	-	-
50MZ+50S+30AS	225	337.5	225	787.5	142.5	285	-	-	-
C+30AS+0.5PEF	225	337.5	225	783.2	142.5	285	4.28	-	-
C+30AS+1PEF	225	337.5	225	774.7	142.5	285	8.55	-	-
C+30AS+1.5PEF	225	337.5	225	761.85	142.5	285	12.82	-	-
C+30AS+2PEF	225	337.5	225	744.75	142.5	285	17.1	-	-
C+30AS+0.5PAF	225	337.5	225	784.09	142.5	285	-	3.41	-
C+30AS+1PAF	225	337.5	225	781.22	142.5	285	-	6.82	-
C+30AS+1.5PAF	225	337.5	225	764.44	142.5	285	-	10.23	-
C+30AS+2PAF	225	337.5	225	748.20	142.5	285	-	13.65	-
C+30AS+0.5BF	225	337.5	225	734.63	142.5	285	-	-	10.12
C+30AS+1BF	225	337.5	225	763.84	142.5	285	-	-	20.25
C+30AS+1.5BF	225	337.5	225	750.85	142.5	285	-	-	30.37
C+30AS+2BF	225	337.5	225	723.94	142.5	285	-	-	40.5

To evaluate the mechanical properties of the AACs, both cubic (50x50x50 mm) and prismatic (40x40x160 mm) samples were prepared. Compressive and flexural strengths were measured using an automatic testing machine following the relevant standards. For water absorption tests, as per ASTM C 642, the oven-dried samples were weighed and then immersed in water for 48 hours to achieve saturation before being reweighed. Flexural strength was assessed on the 28th day using a single-point loading method in a standardized testing setup (Fig. 1.).

Fig. 1. Images of the experimental setup and specimen testing process, including preparation, testing, and storage of AACs.

3. Results and Discussion

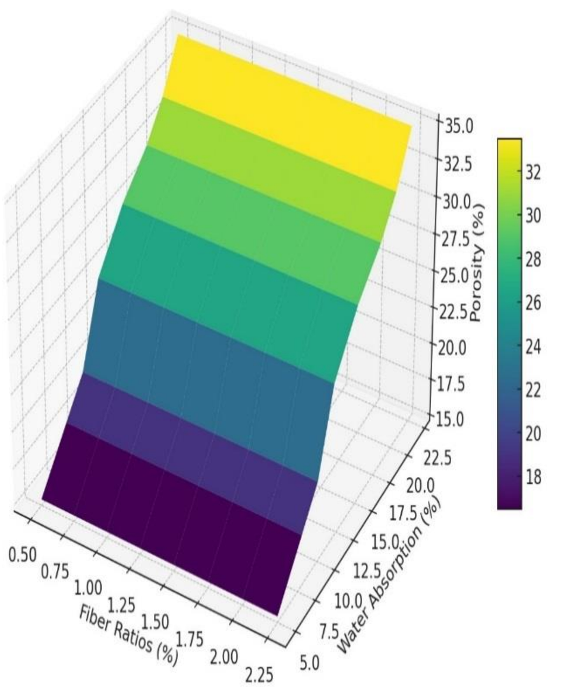

Fig. 2. Water absorption and void ratio values of fiber-reinforced AACs at 28 days.

The detailed analysis of the relationships among fiber ratios, water absorption, and porosity in construction materials provides crucial insights into the behavior of AAC compositions under various fiber concentrations and the inclusion of AS. The observed linear progressions in the fiber ratios versus water absorption and porosity Fig. 2. underline a significant influence of incremental increases in fiber content on these essential material properties, reflecting both opportunities and challenges in material design for construction applications. Starting with the relationship between fiber ratios and water absorption, the upward trajectory from 0.5% to 2.25% fiber content, leading to an increase in water absorption from about 5% to over 22%, highlights a critical point: while increased fiber content enhances certain material properties, it also raises water absorption significantly. This observation is particularly relevant in environments prone to moisture or direct water exposure, where high water absorption could undermine material integrity. However, the graph also suggests a saturation point at around 2.0% fiber ratio, beyond which water absorption does not decrease, indicating a threshold where additional fibers may contribute to increased porosity rather than enhancing water resistance. Regarding porosity, the similarly ascending trend as fiber content increases suggests that higher fiber concentrations may offer benefits such as improved insulation properties or reduced material density but also introduce greater porosity. This increased porosity could weaken the material's structural strength, making it less suitable for load-bearing applications unless compensatory design measures are implemented. However, the optimal fiber ratio, evidenced around 1.0%, effectively balances the dual needs of reduced water absorption and lower porosity, achieving a denser and more robust matrix. Further analysis incorporating 10% and 20% AS in the AAC matrix indicates that these additions significantly reduce water absorption through chemical interactions, likely involving the $CaO/CaSO_4$ composite activator, which promotes the formation of long-chain Si-O-Al-O structures that density the matrix and reduce porosity. Yet, at 30% AS, the benefits diminish as water absorption increases, suggesting a detrimental oversaturation effect that could introduce microstructural weaknesses. BFs merge as particularly effective among various fiber types analyzed, demonstrating the lowest water absorption and porosity across all ratios, indicating their superior reinforcement capabilities within the AAC matrix. PEFs at 1% significantly enhance matrix densification, aligning with findings from Sahin et al. [3], which noted a rapid decrease in porosity at a 0.4% PEF ratio but found diminishing returns at higher concentrations.

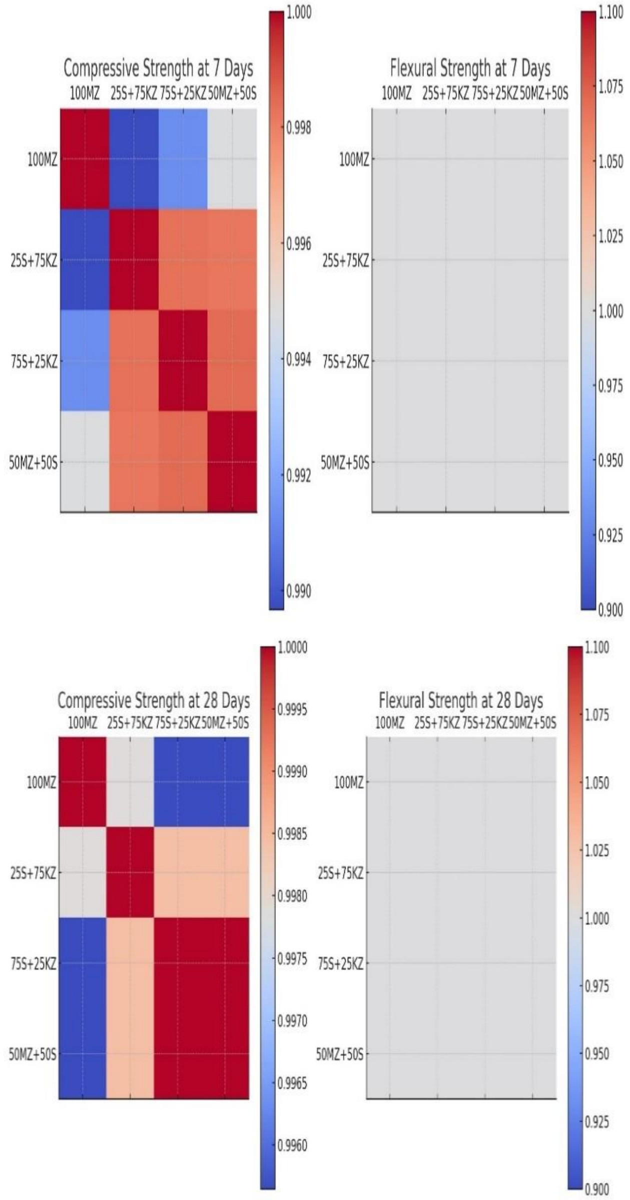

Fig. 3. Compressive and flexural strengths of AACs of different molarity and mixing ratios at 7 and 28 days.

Prior to the commencement of further testing, trial mixtures were prepared with varying compositions and molar ratios. The series exhibiting the highest compressive and flexural strengths was selected for detailed physical and mechanical property evaluations. Subsequent experiments were conducted to investigate the effects of adding 10%, 20%, and 30% AS to the optimized series. Fig. 3. illustrate the anticipated positive correlation between NaOH concentration and compressive and flexural strengths, with peaks observed at 12M before a slight decline at 14M. When subjected to different molarity levels, each of these mixtures demonstrated almost perfect correlation coefficients, indicating highly predictable strength properties under controlled alkaline conditions. At 7 days, the correlation coefficients for compressive strength ranged from 0.989 to 1.000, highlighting an almost uniform rate of chemical reaction and strength development across these varied compositions. This suggests that the initial curing phase rapidly stabilizes material properties, which is crucial for early-stage structural applications. The flexural strength at this early stage also showed perfect correlations (1.0), indicating a uniform resistance to bending forces across all tested mixtures, a critical factor for ensuring the material's reliability in structural components under flexural stress. By 28 days, the materials continued to exhibit strong correlations in compressive strength, with coefficients from 0.995 to 1.000, confirming that the compositions reached a state of chemical equilibrium or full reaction maturity, reflecting the standard industry practice of using a 28-day curing period to assess material strength for structural applications. The perfect correlation in flexural strength across mixtures at 28 days reinforces the materials' consistent performance. It underscores their suitability for diverse construction needs where long-term durability and resistance to mechanical stress are required. This analysis underscores the predictability and reliability of these material mixtures in achieving specified strength characteristics, which are essential for optimizing construction processes and enhancing structural safety. The ability to anticipate how different compositions respond to changes in molarity allows engineers to tailor materials to specific environmental conditions and structural requirements, streamlining construction timelines and potentially reducing costs. Furthermore, this insight into material behavior supports ongoing efforts to refine construction materials for improved performance, ensuring that structures meet and exceed safety and durability standards. Similar trends have been observed by Malkawi et al. [32] and Chaithanya et al. [33] in AACs containing fly ash (FA) or S. These findings are consistent with those of Singh et al. [34] and Mudgal et al. [35], who also identified optimal AS levels for improved strength and compactness in AACs. The presence of AS is conducive to geopolymerization, which likely contributes to a higher Si/Al and Na/Al molar ratio, thereby enhancing densification and strength. Aygörmez [36, 37] reported similar improvements in AAC mortars, achieving a 12% increase in compressive strength with 25% AS replacement. Notably, Zakira et al. [38] achieved even higher strengths (66 MPa) using 50% AS, which highlights the potential of AS for high-performance AACs. The incorporation of AS appears to optimise the internal microstructure of the AACs, promoting a more homogeneous and dense matrix. This densification is of great importance for improving the mechanical properties of the material, as it reduces the number of internal voids and enhances the overall bonding within the material. The findings indicate that AS additions up to 20% result in significant improvements in mechanical performance, in alignment with the studies by Singh et al. [34] and Mudgal et al. [35], which reported similar enhancements in AAC properties with optimal AS levels. Beyond this threshold, at 30% AS, the benefits appear to diminish, likely due to the oversaturation effect, which may lead to increased porosity or the formation of less desirable phases within the matrix. This observation highlights the significance of optimizing the content of supplementary materials, such as AS, to achieve a balance between maximizing strength and maintaining structural integrity. This is consistent with the research by Aygörmez [36, 37], which noted significant long-term strength improvements with AS incorporation. The superior performance of the 75S+25MZ mixture at 12M NaOH can be attributed to several factors, including the optimal dissolution of aluminosilicates, the balanced Na/Al and Si/Al ratios, and the effective densification of the matrix. The presence of slag contributes to long-term strength due to its latent hydraulic properties, which continue to enhance the matrix even after the initial curing period. This is consistent with the findings of Chaithanya et al. [33], who also observed long-term strength gains in AACs with slag. The incorporation of fibers at specific ratios serves to enhance the mechanical properties of the material, as it improves the internal bonding and reduces microcracking. The findings indicate that a 1.0% fiber ratio is optimal for both compressive and flexural strengths, as it provides the most optimal balance between fiber reinforcement and matrix integrity. The positive correlation between NaOH concentration and mechanical properties up to 12M is well-supported by the literature, with similar trends observed in studies by Malkawi et al. [32] and Singh et al. [34]. The observed trend of increasing strength with higher molarity up to 12M is consistent with the findings of Malkawi et al. [32], who reported that higher NaOH concentrations improve the dissolution of aluminosilicate precursors, leading to a denser and stronger matrix. Nevertheless, the slight decline in strength at 14M may be attributed to the excessive alkali content, which may result in the formation of alkali carbonates or other secondary phases that do not contribute to strength development. At 28 days, the compressive strength trends remain consistent with the 7-day results. The 75S+25MZ mixture continues to demonstrate superior performance, achieving compressive strengths exceeding 50 MPa at 12M NaOH. This sustained strength gain over time indicates a stable and ongoing geopolymerization process. The presence of slag in the mixture enhances the long-term strength due to its latent hydraulic properties, which contribute to continued strength development beyond the initial curing period. Similarly, Chaithanya et al. [33] observed comparable long-term strength gains in AACs with S, underscoring the significance of slag content in attaining high-performance composites. Flexural strength is a crucial parameter that reflects the material's capacity to withstand bending and cracking. The flexural strength at seven days follows a similar trend to compressive strength, with the 75S+25MZ mixture exhibiting the highest values. This finding is consistent with the findings of Singh et al. [34], who reported that optimal AS levels and fiber reinforcement significantly enhance the flexural strength of AACs. The 28-day flexural strength results serve to reinforce the superiority of the 75S+25MZ mixture. At 12M NaOH, the flexural strength exceeds 20 MPa, indicating excellent durability and resistance to bending stresses over time. The slight decline observed at 14M molarity is consistent with the compressive strength results, suggesting that excessively high NaOH concentrations may have an adverse effect on the matrix structure. Mudgal et al. [35] also observed that while higher alkali concentrations enhance early strength, they can lead to long-term durability issues if not optimized.

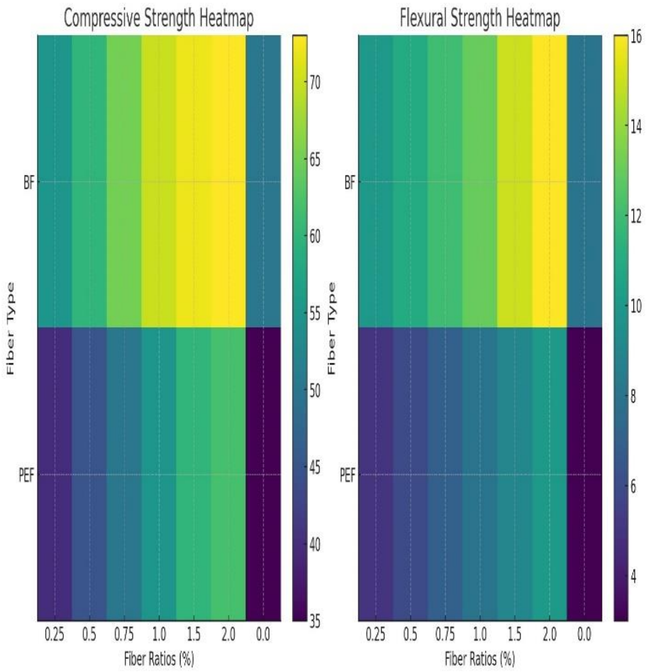

Fig. 4. Compressive and flexural strengths of AACs in different synthetic fibers and ratios at 28 days.

The data presented in Fig. 4 indicates that PEFs were beneficial only up to a 1% addition, achieving a maximum compressive strength of 47.06 MPa before experiencing a significant decline. This decline can be attributed to the phenomenon of fiber agglomeration at higher concentrations, which leads to poor dispersion and the creation of weak points within the matrix. The heatmaps vividly illustrate the compressive and flexural strengths of construction materials integrated with BF and PEFs, providing a clear visual distinction across various fiber ratios from 0.25% to 2.00%, including a control sample without fibers. This analysis serves not only as a comparative overview but also as a deep dive into the material science implications of fiber reinforcement in cementitious composites. Starting with the compressive strength, the heatmap gradients—transitioning from deep purples to vibrant yellows—indicate increasing strength levels as the fiber content rises. Particularly, BFs exhibit superior performance over Polyethylene Fibers, underscored by consistently higher values across all fiber ratios. This distinction could be attributed to the inherent mechanical properties of basalt fibers, which include high tensile strength and stiffness. These properties effectively transfer stress across the fiber-matrix interface, enhancing the composite's overall load-bearing capacity. The presence of basalt fibers potentially initiates a more efficient crack distribution mechanism, which helps in arresting cracks at early stages, thereby improving the compressive strength. On the other hand, PEFs, while still enhancing strength, offer a different set of benefits and challenges. These synthetic fibers are known for their flexibility and high strain capacity, which contribute positively to the energy absorption capabilities and toughness of the concrete. However, their lower modulus compared to basalt fibers might explain the lesser improvement in compressive strength, as they do not contribute as effectively to the stiffness of the composite. Nevertheless, their inclusion in the composite matrix still offers valuable enhancements, particularly in applications where flexibility and impact resistance are desirable. The flexural strength heatmap further explores the dynamic between fiber content and bending resistance. Again, the visual gradient reflects an increase in strength with higher fiber ratios, with BFs leading in performance enhancement. In flexural applications, the role of fibers is critical as they bridge cracks that might otherwise propagate under bending stress, thereby maintaining the integrity of the material under load. The effective distribution and bonding of basalt fibers within the matrix can significantly increase the material's resistance to bending, highlighting their suitability for structural applications where flexural stresses are prevalent. The control samples, noticeably lower in strength in both heatmaps, underscore the significant role that fibers play in enhancing concrete properties. The contrast between the fiber-enhanced samples and the control illustrates the effectiveness of fiber integration, providing a stark visualization of the material advancements achievable through fiber technology. Similarly, Uysal et al. [39] observed enhancements in mechanical properties with various fibers in AS-MK-AACs. The researchers observed that PVAFs effectively increased flexural strength by 61% compared to the control, indicating the potential of synthetic fibers in enhancing AACs' mechanical performance. The enhanced performance of BFs can be attributed to their intrinsic properties and the synergistic interactions with the AAC matrix. BFs, derived from volcanic rock, exhibit excellent mechanical properties, including high tensile strength, chemical resistance, and thermal stability. These properties render BFs particularly suitable for reinforcing AACs, as they can withstand the alkaline environment and high temperatures associated with geopolymerization. The compatibility of BFs with the AAC matrix ensures effective stress transfer and crack bridging, which results in significant improvements in compressive strength. The fiber bridging effect, whereby fibers span across cracks and transfer stress, plays a pivotal role in regulating crack formation and development. As the fibers bridge the cracks, they effectively arrest crack growth and enhance the load-bearing capacity of the AACs. The flexural strength of the composites increased modestly with fiber reinforcement, with an improvement of approximately 0.5% observed for both PEF and PAF at a fiber content of 0.5%. However, the incorporation of BF at the same 0.5% ratio yielded a substantial improvement of 12.61%, which highlights the superior reinforcing capabilities of BFs. It is noteworthy that when the PEF content was increased to 1%, the flexural strength exhibited a higher value of 10.54 MPa. Notwithstanding this increase, the strength remained below the control value of 12.34 MPa. This trend indicates that while PEFs can enhance flexural strength at certain ratios, they may not be as effective as other types of fibers, such as BF, especially at higher concentrations. The observed pattern of initial strength increase followed by a decline at higher fiber contents is consistent with findings from other studies, including those by Alomayri et al. [40, 41], who investigated cotton fiber-reinforced FA-based AACs (FA-AACs). A similar trend was observed, whereby the flexural strength initially increased with fiber content up to 0.5%, but declined beyond this point. This behavior can be attributed to optimal fiber dispersion at lower ratios, which facilitates effective stress transfer. In contrast, higher fiber contents can lead to agglomeration and inhomogeneous distribution within the matrix. The superior performance of BF at 0.5% can be attributed to its intrinsic mechanical properties and its interaction with the geopolymer matrix. Basalt fibers are renowned for their high tensile strength, excellent chemical resistance, and thermal stability, rendering them optimal for reinforcing AACs. The robust bond between BFs and the AAC matrix ensures efficient stress transfer and crack bridging, significantly enhancing the material's flexural strength. This is corroborated by the findings of Baykara et al. [42], who observed that PPF-reinforced AACs also exhibited optimal performance at 0.5% fiber content. Beyond this optimal ratio, the performance declined due to potential issues such as fiber inhomogeneity and agglomeration, which compromise the matrix integrity and lead to the formation of weak points.

4. Conclusions

In the exploration of optimized AACs, the study reveals significant enhancements in mechanical properties through various additives and modifications. AAC mixture comprising 50% MZand 50% S, augmented with 30% AS at a 12M NaOH concentration, exhibited an exceptional compressive strength of 61.85 MPa, demonstrating the efficacy of high molarity and specialized components in achieving superior strength. Furthermore, the addition of BFs at just a 0.5% ratio not only increased the compressive strength by 7.26% but also significantly boosted the flexural strength by 24.15%, highlighting BF's remarkable reinforcing capabilities. Conversely, PEFs, used at a 1% ratio, enhanced the flexural strength to 10.54 MPa, yet this figure still fell below the control mix's strength, indicating a nuanced interplay between fiber type and concentration in AAC performance. Additionally, the mixture of 75% Slag with 25% Metazeolite consistently showed the highest compressive strength across all tested molarity levels, particularly achieving around 50 MPa at a 12M NaOH concentration within 7 days. This composition maintained its peak strength over 28 days, underscoring its robustness. However, an increase in Aluminum Sludge content to 30% resulted in higher water absorption, suggesting a threshold beyond which additional AS is counterproductive. This intricate study not only underscores the importance of precise component ratios and types in AAC but also provides a roadmap for tailoring AAC properties to meet specific structural requirements effectively.

References

[1] M. Lakew, O. Canpolat, M. M. Al-Mashhadani, M. Uysal, A. Niş, Y. Aygörmez and M. Bayati, "Combined effect of using steel fibers and demolition waste aggregates on the performance of fly ash/slag based geopolymer concrete," *European Journal of Environmental and Civil Engineering,* pp. 1-28, 3 2023.

[2] Ş. O. Demirel C., "Erken Yaşdaki Atık Betonların Geri Dönüşüm Agregası Olarak Beton Üretiminde Kullanılabilirliği ve Sürdürülebilirlik Açısından İncelenmesi.," *Düzce Üniversitesi Bilim ve Teknoloji Dergisi,,* no. 3, pp. 226-235, 2015.

[3] F. Sahin, M. Uysal, O. Canpolat, T. Cosgun and H. Dehghanpour, "The effect of polyvinyl fibers on metakaolin-based geopolymer mortars with different aggregate filling," *Construction and Building Materials,* vol. 300, 9 2021.

[4] X. Zheng, J. Zhang, X. Ding, H. Chu and J. Zhang, "Frost resistance of internal curing concrete with calcined natural zeolite particles," *Construction and Building Materials,* vol. 288, 6 2021.

[5] C. Florez, O. Restrepo-Baena and J. I. Tobon, "Effects of calcination and milling pre-treatments on natural zeolites as a supplementary cementitious material," *Construction and Building Materials,* vol. 310, 12 2021.

[6] A. Nikolov, H. Nugteren and I. Rostovsky, "Optimization of geopolymers based on natural zeolite clinoptilolite by calcination and use of aluminate activators," *Construction and Building Materials,* vol. 243, 5 2020.

[7] S. Özen and B. Alam, "Compressive strength and microstructural characteristics of natural zeolite-based geopolymer," *Periodica Polytechnica Civil Engineering,* vol. 62, no. 1, pp. 64-71, 2018.

[8] Y. Aygörmez, "Performance of ambient and freezing-thawing cured metazeolite and slag based geopolymer composites against elevated temperatures," *Revista de la Construccion,* vol. 20, no. 1, pp. 145-162, 2021.

[9] R. R. Bellum, "Influence of steel and PP fibers on mechanical and microstructural properties of fly ash-GGBFS based geopolymer composites," *Ceramics International,* vol. 48, no. 5, pp. 6808-6818, 3 2022.

[10] O.Abdulkareem and J. Matthews, "Improving the Mechanical Strengths of Hybrid Waste Geopolymer Binders by Short Fiber Reinforcement," *Arabian Journal for Science and Engineering,* vol. 46, no. 5, pp. 4781-4789, 2021.

[11] Y. Alrefaei and J.-G. Dai, "Tensile behavior and microstructure of hybrid fiber ambient cured one-part engineered geopolymer composites," *Construction and Building Materials,* vol. 184, pp. 419-431, 2018.

[12] F. Amalia, N. Akifah, Nurfadilla and Subaer, "Development of coconut trunk fiber geopolymer hybrid composite for structural engineering materials," *IOP Conference Series: Materials Science and Engineering,* vol. 180, no. 1, 2017.

[13] K. Arunkumar, M. Muthukannan, A. Sureshkumar, A. Chithambarganesh and R. Rangaswamy Kanniga Devi, "Mechanical and durability characterization of hybrid fibre reinforced green geopolymer concrete," *Research on Engineering Structures and Materials,* vol. 8, no. 1, pp. 19-43, 2022.

[14] P. Nuaklong, A. Wongsa, K. Boonserm, C. Ngohpok, P. Jongvivatsakul, V. Sata, P. Sukontasukkul and P. Chindaprasirt, "Enhancement of mechanical properties of fly ash geopolymer containing fine recycled concrete aggregate with micro carbon fiber," *Journal of Building Engineering,* vol. 41, 9 2021.

[15] W. Punurai, W. Kroehong, A. Saptamongkol and P. Chindaprasirt, "Mechanical properties, microstructure and drying shrinkage of hybrid fly ash-basalt fiber geopolymer paste," *Construction and Building Materials,* vol. 186, pp. 62-70, 2018.

[16] W. H. Sachet and W. D. Salman, "Compressive Strength Development of Slag-Based Geopolymer Paste Reinforced with Fibers Cured at Ambient Condition," *IOP Conference Series: Materials Science and Engineering,* vol. 928, no. 2, 11 2020.

[17] K. Zada Farhan, M. Azmi Megat Johari and R. Demirboğa, "Evaluation of properties of steel fiber reinforced GGBFS-based geopolymer composites in aggressive environments," *Construction and Building Materials,* vol. 345, p. 128339, 8 2022.

[18] M. Frydrych, S. Hýsek, L. Fridrichová, S. Van, M. Herclík, M. Pechociaková, H. Chi and P. Louda, "Impact of flax and basalt fibre reinforcement on selected properties of geopolymer composites," *Sustainability (Switzerland),* vol. 12, no. 1, 2020.

[19] X. Gao, Q. Yu, R. Yu and H. Brouwers, "Evaluation of hybrid steel fiber reinforcement in high performance geopolymer composites," *Materials and Structures/Materiaux et Constructions,* vol. 50, no. 2, 2017.

[20] S. Guler and Z. F. Akbulut, "Effect of high-temperature on the behavior of single and hybrid glass and basalt fiber added geopolymer cement mortars," *Journal of Building Engineering,* vol. 57, p. 104809, 10 2022.

[21] C. Le, P. Louda, K. Buczkowska and I. Dufkova, "Investigation on flexural behavior of geopolymer-based carbon textile/basalt fiber hybrid composite," *Polymers,* vol. 13, no. 5, pp. 1-18, 2021.

[22] V. Sathish Kumar, N. Ganesan and P. Indira, "Effect of hybrid fibres on the durability characteristics of ternary blend geopolymer concrete," *Journal of Composites Science,* vol. 5, no. 10, 2021.

[23] A. Baziak, K. Pławecka, I. Hager, A. Castel and K. Korniejenko, "Development and characterization of lightweight geopolymer composite reinforced with hybrid carbon and steel," *Materials,* vol. 14, no. 19, 2021.

[24] A. Chithambar Ganesh and M. Muthukannan, "Experimental Study on the Behaviour of Hybrid Fiber Reinforced Geopolymer Concrete under Ambient Curing Condition," *IOP Conference Series: Materials Science and Engineering,* vol. 561, no. 1, 11 2019.

[25] D. Jia, P. He, M. Wang and S. Yan, Short SiC Fiber and Hybrid SiC/Carbon Fiber Reinforced Geopolymer Matrix Composites, vol. 311, 2020, pp. 243-270. 10.1007/978-981-15-9536-3_7.

[26] J. Junior, A. Saha, P. Sarker and A. Pramanik, "Workability and flexural properties of fibre-reinforced geopolymer using different mono and hybrid fibres," *Materials,* vol. 14, no. 16, 2021.

[27] M. Maras, "Tensile and flexural strength cracking behavior of geopolymer composite reinforced with hybrid fibers," *Arabian Journal of Geosciences,* vol. 14, no. 22, 2021.

[28] P. Sukontasukkul, P. Pongsopha, P. Chindaprasirt and S. Songpiriyakij, "Flexural performance and toughness of hybrid steel and polypropylene fibre reinforced geopolymer," *Construction and Building Materials,* vol. 161, pp. 37-44, 2 2018.

[29] N. P. Asrani, G. Murali, K. Parthiban, K. Surya, A. Prakash, K. Rathika and U. Chandru, "A feasibility of enhancing the impact resistance of hybrid fibrous geopolymer composites: Experiments and modelling," *Construction and Building Materials,* vol. 203, pp. 56-68, 4 2019.

[30] J. I. Choi, H. H. Nguyễn, S. E. Park, R. Ranade and B. Y. Lee, "Effects of fiber hybridization on mechanical properties and autogenous healing of alkali-activated slag-based composites," *Construction and Building Materials,* vol. 310, 12 2021.

[31] F. U. A. Shaikh, "Tensile and flexural behaviour of recycled polyethylene terephthalate (PET) fibre reinforced geopolymer composites," *Construction and Building Materials,* vol. 245, 6 2020.

[32] A. B. Malkawi, M. F. Nuruddin, A. Fauzi, H. Almattarneh and B. S. Mohammed, "Effects of Alkaline Solution on Properties of the HCFA

Geopolymer Mortars," *Procedia Engineering,* vol. 148, pp. 710-717, 2016.

[33] R. K. Chaithanya, C. V. Reddy, L. S. Reddy and K. T. Kumar, "Effect Of Molarity On Strength Characteristics Of Geopolymer Mortar Based On Fly ash and GGBS". *Solid State Technology.* (2020), 63(2s).

[34] S. Singh, M. U. Aswath and R. V. Ranganath, "Performance assessment of bricks and prisms: Red mud based geopolymer composite," *Journal of Building Engineering,* vol. 32, 11 2020.

[35] M. Mudgal, A. Singh, R. K. Chouhan, A. Acharya and A. K. Srivastava, "Fly ash red mud geopolymer with improved mechanical strength," *Cleaner Engineering and Technology,* vol. 4, 10 2021.

[36] Y.Aygörmez, "Assessment of performance of metabentonite and metazeolite-based geopolymers with fly ash sand replacement," *Construction and Building Materials,* vol. 302, 10 2021.

[37] Y. Aygörmez, "Evaluation of the red mud and quartz sand on reinforced metazeolite-based geopolymer composites," *Journal of Building Engineering,* vol. 43, 11 2021.

[38] U.Zakira, K. Zheng, N. Xie and B.Birgisson, "Development of high-strength geopolymers from red mud and blast furnace slag," *Jour. of Clean. Prod,* vol. 383, 1 2023.

[39] M. Uysal, Ö. Faruk Kuranlı, Y. Aygörmez, O. Canpolat and T. Çoşgun, "The effect of various fibers on the red mud additive sustainable geopolymer composites," *Cons. and Buil. Mat,* vol. 363, 1 2023.

[40] T. Alomayri and I. M. Low, "Synthesis and characterization of mechanical properties in cotton fiber-reinforced geopolymer composites," *Journal of Asian Ceramic Societies,* vol. 1, no. 1, pp. 30-34, 2013.

[41] T. Alomayri, F. U. Shaikh and I. M. Low, "Characterisation of cotton fibre-reinforced geopolymer composites," *Composites Part B: Engineering,* vol. 50, pp. 1-6, 7 2013.

[42] H. Baykara, M. H. Cornejo, A. Espinoza, E. García and N. Ulloa, "Preparation, characterization, and evaluation of compressive strength of PFRGM," *Heliyon,* vol. 6, no. 4, 4 2020.

INTERNATIONAL JOURNAL OF ENGINEERING TECHNOLOGIES-IJET

Guide for Authors

The **International Journal of Engineering Technologies (IJET)** seeks to promote and disseminate knowledge of the various topics of engineering technologies. The journal aims to present to the international community important results of work in the fields of engineering such as imagining, researching, planning, creating, testing, improving, implementing, using and asking. The journal also aims to help researchers, scientists, manufacturers, institutions, world agencies, societies, etc. to keep up with new developments in theory and applications and to provide alternative engineering solutions to current.

The *International Journal of Engineering Technologies* is a quarterly published journal and operates an online submission and peer review system allowing authors to submit articles online and track their progress via its web interface. The journal aims for a publication speed of **60 days** from submission until final publication.

The coverage of IJET includes the following engineering areas, but not limited to:

All filed of engineering such as;

Chemical engineering

- Biomolecular engineering
- Materials engineering
- Molecular engineering
- Process engineering

Civil engineering

- Environmental engineering
- Geotechnical engineering
- Structural engineering
- Transport engineering
- Water resources engineering

Electrical engineering

- Computer engineering
- Electronic engineering
- Optical engineering
- Power engineering

Mechanical engineering

- Acoustical engineering
- Manufacturing engineering
- Thermal engineering
- Vehicle engineering

Systems (interdisciplinary) engineering

- Aerospace engineering
- Agricultural engineering
- Applied engineering
- Biological engineering
- Building services engineering
- Energy engineering
- Railway engineering
- Industrial engineering
- Mechatronics
- Military engineering
- Nano engineering
- Nuclear engineering
- Petroleum engineering

Types of Articles submitted should be original research papers, not previously published, in one of the following categories,

- Applicational and design studies.
- Technology development,

– Comparative case studies.

– Reviews of special topics.

– Reviews of work in progress and facilities development.

– Survey articles.

– Guest editorials for special issues.

Ethic Responsibilities

The publication of an article in peer-reviewed *"International Journal of Engineering Technologies"* is an essential building block in the development of a coherent and respected network of knowledge. It is a direct reflection of the quality of the work. Peer-reviewed articles support and embody the scientific method. It is therefore important to agree upon standards of expected ethical behavior for all parties involved in the act of publishing: the author, the journal editor, the peer reviewer, the publisher and the society of society-owned or sponsored journals.

All authors are requested to disclose any actual or potential conflict of interest including any financial, personal or other relationships with other people or organizations within three years of beginning the submitted work that could inappropriately influence, or be perceived to influence, their work.

Submission of an article implies that the work described has not been published previously that it is not under consideration for publication elsewhere. The submission should be approved by all authors and tacitly or explicitly by the responsible authorities where the work was carried out, and that, if accepted, it will not be published elsewhere in the same form, in English or in any other language, including electronically without the written consent of the copyright-holder.

Upon acceptance of an article, authors will be asked to complete a "Copyright Form". Acceptance of the agreement will ensure the widest possible dissemination of information. An e-mail will be sent to the corresponding author confirming receipt of the manuscript together with a "Copyright Form" form or a link to the online version of this agreement.

Author Rights

As a journal author, you retain rights for a large number of author uses, including use by your employing institute or company. These rights are retained and permitted without the need to obtain specific permission from *IJET*. These include:

- The right to make copies (print or electronic) of the journal article for your own personal use, including for your own classroom teaching use;
- The right to make copies and distribute copies (including via e-mail) of the journal article to research colleagues, for personal use by such colleagues for scholarly purposes;
- The right to post a pre-print version of the journal article on internet web sites including electronic pre-print servers, and to retain indefinitely such version on such servers or sites for scholarly purposes
- the right to post a revised personal version of the text of the final journal article on your personal or institutional web site or server for scholarly purposes
- The right to use the journal article or any part thereof in a printed compilation of your works, such as collected writings or lecture notes.

Article Style

Authors must strictly follow the guide for authors, or their articles may be rejected without review. Editors reserve the right to adjust the style to certain standards of uniformity. Follow Title, Authors, Affiliations, Abstract, Keywords, Introduction, Materials and Methods, Theory/Calculation, Conclusions, Acknowledgements, References order when typing articles. The corresponding author should be identified with an asterisk and footnote. Collate acknowledgements in a separate section at the end of the article and do not include them on the title page, as a footnote to the title or otherwise.

Abstract and Keywords:

Enter an abstract of up to 250 words for all articles. This is a concise summary of the whole paper, not just the conclusions, and is understandable without reference to the rest of the paper. It should contain no citation to other published work. Include up to six keywords that describe your paper for indexing purposes.

Abbreviations and Acronyms:

Define abbreviations and acronyms the first time they are used in the text, even if they have been defined in the abstract. Abbreviations such as IEEE, SI, MKS, CGS, sc, dc, and rms do not have to be defined. Do not use abbreviations in the title unless they are unavoidable.

Text Layout for Peer Review:

Use single column layout, double spacing and wide (3 cm) margins on white paper at the peer review stage. Ensure that each new paragraph is clearly indicated. Present tables and figure legends in the text where they are related and cited. Number all pages consecutively; use 12 pt font size and standard fonts; Times New Roman, Helvetica, or Courier is preferred.

Research Papers should not exceed 12 printed pages in two-column publishing format, including figures and tables.

Technical Notes and *Letters* should not exceed 2,000 words.

Reviews should not exceed 20 printed pages in two-column publishing format, including figures and tables.

Equations:

Number equations consecutively with equation numbers in parentheses flush with the right margin, as in (1). To make equations more compact, you may use the solidus (/), the exp function, or appropriate exponents. Italicize Roman symbols for quantities and variables, but not Greek symbols. Use an dash (–) rather than a hyphen for a minus sign. Use parentheses to avoid ambiguities in denominators. Punctuate equations with commas or periods when they are part of a sentence, as in

$$C = a + b \qquad (1)$$

Symbols in your equation should be defined before the equation appears or immediately following. Use “Eq. (1)” or “equation (1),” while citing.

Figures and Tables:

All illustrations must be supplied at the correct resolution:

* Black and white and colour photos - 300 dpi

* Graphs, drawings, etc - 800 dpi preferred; 600 dpi minimum

* Combinations of photos and drawings (black and white and color) - 500 dpi

In addition to using figures in the text, upload each figure as a separate file in either .tiff or .eps format during submission, with the figure number.

Table captions should be written in the same format as figure captions; for example, “Table 1. Appearance styles.”. Tables should be referenced in the text unabbreviated as “Table 1.”

References:

Please ensure that every reference cited in the text is also present in the reference list (and viceversa). Any references cited in the abstract must be given in full. Unpublished results and personal communications are not recommended in the reference list, but may be mentioned in the text. Citation of a reference as “in press” implies that the item has been accepted for publication. Number citations consecutively in square brackets [1]. Punctuation follows the bracket [2]. Refer simply to the reference number, as in [3]. Use “Ref. [3]” or Reference [3]” at the beginning of a sentence: “Reference [3] was …”. Give all authors’ names; use “et al.” if there are six authors or more. For papers published in translated journals, first give the English citation, then the original foreign-language citation.

Books

[1] J. Clerk Maxwell*, A Treatise on Electricity and Magnetism,* 3rd ed., vol. 2. Oxford:Clarendon Press, 1892, pp.68-73.

Journals

[2] Y. Yorozu, M. Hirano, K. Oka, and Y. Tagawa, “Electron spectroscopy studies on magneto-optical media and plastic substrate interface”, *IEEE Transl. J. Magn. Japan*, vol. 2, pp. 740-741, August 1987.

Conferences

[3] Çolak I., Kabalci E., Bayindir R., and Sagiroglu S, “The design and analysis of a 5-level cascaded voltage source inverter with low THD”, *2nd PowerEng Conference*, Lisbon, pp. 575-580, 18-20 March 2009.

Reports

[4] IEEE Standard 519-1992, Recommended practices and requirements for harmonic control in electrical power systems, *The Institute of Electrical and Electronics Engineers*, 1993.

Text Layout for Accepted Papers:

A4 page margins should be margins: top = 24 mm, bottom = 24 mm, side = 15 mm. Main text should be given in two column. The column width is 87mm (3.425 in). The space between the two columns is 6 mm (0.236 in). Paragraph indentation is 3.5 mm (0.137 in). Follow the type sizes specified in Table. Position figures and tables at the tops and bottoms of columns. Avoid placing them in the middle of columns. Large figures and tables may span across both columns. Figure captions should be centred below the figures; table captions should be centred above. Avoid placing figures and tables before their first mention in the text. Use the abbreviation “Fig. 1,” even at the beginning of a sentence.

Type size (pts.)	Appearance		
	Regular	**Bold**	*Italic*
10	Authors' affiliations, Section titles, references, tables, table names, first letters in table captions,figure captions, footnotes, text subscripts, and superscripts	**Abstract**	
12	Main text, equations, Authors' names, [a]		*Subheading (1.1.)*
24	Paper title		

Submission checklist:

It is hoped that this list will be useful during the final checking of an article prior to sending it to the journal's Editor for review. Please consult this Guide for Authors for further details of any item. Ensure that the following items are present:

- ❖ One Author designated as corresponding Author:

• E-mail address

• Full postal address

• Telephone and fax numbers

- ❖ All necessary files have been uploaded

• Keywords: a minimum of 4

• All figure captions (supplied in a separate document)

• All tables (including title, description, footnotes, supplied in a separate document)

- ❖ Further considerations

• Manuscript has been "spellchecked" and "grammar-checked"

• References are in the correct format for this journal

• All references mentioned in the Reference list are cited in the text, and vice versa

• Permission has been obtained for use of copyrighted material from other sources (including the Web)

• Color figures are clearly marked as being intended for color reproduction on the Web (free of charge) and in print or to be reproduced in color on the Web (free of charge) and in black-and-white in print.

Article Template Containing Author Guidelines for Peer-Review

First Author*, Second Author**‡, Third Author***

*Department of First Author, Faculty of First Author, Affiliation of First Author, Postal address

**Department of Second Author, Faculty of First Author, Affiliation of First Author, Postal address

***Department of Third Author, Faculty of First Author, Affiliation of First Author, Postal address

(First Author Mail Address, Second Author Mail Address, Third Author Mail Address)

‡ Corresponding Author; Second Author, Postal address, Tel: +90 312 123 4567, Fax: +90 312 123 4567,corresponding@affl.edu

Received: xx.xx.xxxx Accepted:xx.xx.xxxx

Abstract- Enter an abstract of up to 250 words for all articles. This is a concise summary of the whole paper, not just the conclusions, and is understandable without reference to the rest of the paper. It should contain no citation to other published work. Include up to six keywords that describe your paper for indexing purposes. Define abbreviations and acronyms the first time they are used in the text, even if they have been defined in the abstract. Abbreviations such as IEEE, SI, MKS, CGS, sc, dc, and rms do not have to be defined. Do not use abbreviations in the title unless they are unavoidable.

Keywords- Keyword1; keyword2; keyword3; keyword4; keyword5.

2. Introduction

Authors should any word processing software that is capable to make corrections on misspelled words and grammar structure according to American or Native English. Authors may get help by from word processor by making appeared the paragraph marks and other hidden formatting symbols. This sample article is prepared to assist authors preparing their articles to IJET.

Indent level of paragraphs should be 0.63 cm (0.24 in) in the text of article. Use single column layout, double-spacing and wide (3 cm) margins on white paper at the peer review stage. Ensure that each new paragraph is clearly indicated. Present tables and figure legends in the text where they are related and cited. Number all pages consecutively; use 12 pt font size and standard fonts; Times New Roman, Helvetica, or Courier is preferred. Indicate references by number(s) in square brackets in line with the text. The actual authors can be referred to, but the reference number(s) must always be given. Example: "..... as demonstrated [3, 6]. Barnaby and Jones [8] obtained a different result ...."

IJET accepts submissions in three styles that are defined as Research Papers, Technical Notes and Letter, and Review paper. The requirements of paper are as listed below:

- Research Papers should not exceed 12 printed pages in two-column publishing format, including figures and tables.
- Technical Notes and Letters should not exceed 2,000 words.
- Reviews should not exceed 20 printed pages in two-column publishing format, including figures and tables.

Authors are requested write equations using either any mathematical equation object inserted to word processor or using independent equation software. Symbols in your equation should be defined before the equation appears or immediately following. Use “Eq. (1)” or “equation (1),” while citing. Number equations consecutively with equation numbers in parentheses flush with the right margin, as in Eq. (1). To make equations more compact, you may use the solidus (/), the exp function, or appropriate exponents. Italicize Roman symbols for quantities and variables, but not Greek symbols. Use an dash (–) rather than a hyphen for a minus sign. Use parentheses to avoid ambiguities in denominators. Punctuate equations with commas or periods when they are part of a sentence, as in

$$C = a + b \qquad (1)$$

Section titles should be written in bold style while sub section titles are italic.

3. Figures and Tables

3.1. Figure Properties

All illustrations must be supplied at the correct resolution:

- Black and white and colour photos - 300 dpi
- Graphs, drawings, etc - 800 dpi preferred; 600 dpi minimum
- Combinations of photos and drawings (black and white and colour) - 500 dpi

In addition to using figures in the text, Authors are requested to upload each figure as a separate file in either .tiff or .eps format during submission, with the figure number as Fig.1., Fig.2a and so on. Figures are cited as "Fig.1" in sentences or as "Figure 1" at the beginning of sentence and paragraphs. Explanations related to figures should be given before figure. Figures and tables should be located at the top or bottom side of paper as done in accepted article format.

Figure 1. Engineering technologies.

Table captions should be written in the same format as figure captions; for example, "Table 1. Appearance styles.". Tables should be referenced in the text unabbreviated as "Table 1."

Table 1. Appearance properties of accepted manuscripts

Type size (pts.)	Appearance		
	Regular	**Bold**	*Italic*
10	Authors' affiliations, Abstract, keywords, references, tables, table names, figure captions, footnotes, text subscripts, and superscripts	**Abstract**	
12	Main text, equations, Authors' names, Section titles		*Subheading (1.1.)*
24	Paper title		

4. Submission Process

The *International Journal of Engineering Technologies* operates an online submission and peer review system that allows authors to submit articles online and track their progress via a web interface. Articles that are prepared referring to this template should be controlled according to submission checklist given in "Guide f Authors". Editor handles submitted articles to IJET primarily in order to control in terms of compatibility to aims and scope of Journal.

Articles passed this control are checked for grammatical and template structures. If article passes this control too, then reviewers are assigned to article and Editor gives a reference number to paper. Authors registered to online submission system can track all these phases.

Editor also informs authors about processes of submitted article by e-mail. Each author may also apply to Editor via online submission system to review papers related to their study areas. Peer review is a critical element of publication, and one of the major cornerstones of the scientific process. Peer Review serves two key functions:

- Acts as a filter: Ensures research is properly verified before being published
- Improves the quality of the research

5. Conclusion

The conclusion section should emphasize the main contribution of the article to literature. Authors may also explain why the work is important, what are the novelties or possible applications and extensions. Do not replicate the abstract or sentences given in main text as the conclusion.

Acknowledgements

Authors may acknowledge to any person, institution or department that supported to any part of study.

References

[1] J. Clerk Maxwell, *A Treatise on Electricity and Magnetism*, 3rd ed., vol. 2. Oxford:Clarendon Press, 1892, pp.68-73. (Book)

[2] H. Poor, *An Introduction to Signal Detection and Estimation*, New York: Springer-Verlag, 1985, ch. 4. (Book Chapter)

[3] Y. Yorozu, M. Hirano, K. Oka, and Y. Tagawa, "Electron spectroscopy studies on magneto-optical media and plastic substrate interface", *IEEE Transl. J. Magn. Japan*, vol. 2, pp. 740-741, August 1987. (Article)

[4] E. Kabalcı, E. Irmak, I. Çolak, "Design of an AC-DC-AC converter for wind turbines", *International Journal of Energy Research*, Wiley Interscience, DOI: 10.1002/er.1770, Vol. 36, No. 2, pp. 169-175. (Article)

[5] I. Çolak, E. Kabalci, R. Bayindir R., and S. Sagiroglu, "The design and analysis of a 5-level cascaded voltage source inverter with low THD", *2nd PowerEng Conference*, Lisbon, pp. 575-580, 18-20 March 2009. (Conference Paper)

[6] IEEE Standard 519-1992, Recommended practices and requirements for harmonic control in electrical power systems, *The Institute of Electrical and Electronics Engineers*, 1993. (Standards and References)

Article Template Containing Author Guidelines for Accepted Papers

First Author*, Second Author**[‡], Third Author***

*Department of First Author, Faculty of First Author, Affiliation of First Author, Postal address

**Department of Second Author, Faculty of First Author, Affiliation of First Author, Postal address

***Department of Third Author, Faculty of First Author, Affiliation of First Author, Postal address

(First Author Mail Address, Second Author Mail Address, Third Author Mail Address)

[‡] Corresponding Author; Second Author, Postal address, Tel: +90 312 123 4567,

Fax: +90 312 123 4567,corresponding@affl.edu

Received: xx.xx.xxxx Accepted:xx.xx.xxxx

Abstract- Enter an abstract of up to 250 words for all articles. This is a concise summary of the whole paper, not just the conclusions, and is understandable without reference to the rest of the paper. It should contain no citation to other published work. Include up to six keywords that describe your paper for indexing purposes. Define abbreviations and acronyms the first time they are used in the text, even if they have been defined in the abstract. Abbreviations such as IEEE, SI, MKS, CGS, sc, dc, and rms do not have to be defined. Do not use abbreviations in the title unless they are unavoidable.

Keywords Keyword1, keyword2, keyword3, keyword4, keyword5.

1. Introduction

Authors should any word processing software that is capable to make corrections on misspelled words and grammar structure according to American or Native English. Authors may get help by from word processor by making appeared the paragraph marks and other hidden formatting symbols. This sample article is prepared to assist authors preparing their articles to IJET.

Indent level of paragraphs should be 0.63 cm (0.24 in) in the text of article. Use single column layout, double-spacing and wide (3 cm) margins on white paper at the peer review stage. Ensure that each new paragraph is clearly indicated. Present tables and figure legends in the text where they are related and cited. Number all pages consecutively; use 12 pt font size and standard fonts; Times New Roman, Helvetica, or Courier is preferred. Indicate references by number(s) in square brackets in line with the text. The actual authors can be referred to, but the reference number(s) must always be given. Example: "..... as demonstrated [3,6]. Barnaby and Jones [8] obtained a different result ...."

IJET accepts submissions in three styles that are defined as Research Papers, Technical Notes and Letter, and Review paper. The requirements of paper are as listed below:

- Research Papers should not exceed 12 printed pages in two-column publishing format, including figures and tables.
- Technical Notes and Letters should not exceed 2,000 words.
- Reviews should not exceed 20 printed pages in two-column publishing format, including figures and tables.

Authors are requested write equations using either any mathematical equation object inserted to word processor or using independent equation software. Symbols in your equation should be defined before the equation appears or immediately following. Use “Eq. (1)” or “equation (1),” while citing. Number equations consecutively with equation numbers in parentheses flush with the right margin, as in Eq. (1). To make equations more compact, you may use the solidus (/), the exp function, or appropriate exponents. Italicize Roman symbols for quantities and variables, but not Greek symbols. Use an dash (-) rather than a hyphen for a minus sign. Use parentheses to avoid ambiguities in denominators. Punctuate equations with commas or periods when they are part of a sentence, as in

$$C = a + b \quad (1)$$

Section titles should be written in bold style while sub section titles are italic.

6. Figures and Tables

6.1. Figure Properties

All illustrations must be supplied at the correct resolution:

- Black and white and colour photos - 300 dpi
- Graphs, drawings, etc - 800 dpi preferred; 600 dpi minimum
- Combinations of photos and drawings (black and white and colour) - 500 dpi

In addition to using figures in the text, Authors are requested to upload each figure as a separate file in either .tiff or .eps format during submission, with the figure number as Fig.1., Fig.2a and so on. Figures are cited as "Fig.1" in sentences or as "Figure 1" at the beginning of sentence and paragraphs. Explanations related to figures should be given before figure.

Fig. 1. Engineering technologies.

Figures and tables should be located at the top or bottom side of paper as done in accepted article format. Table captions should be written in the same format as figure captions; for example, "Table 1. Appearance styles.". Tables should be referenced in the text unabbreviated as "Table 1."

Table 1. Appearance properties of accepted manuscripts

Type size (pts.)	Appearance		
	Regular	**Bold**	*Italic*
10	Main text, section titles, authors' affiliations, abstract, keywords, references, tables, table names, figure captions, equations, footnotes, text subscripts, and superscripts	**Abstract-**	*Subheading (1.1.)*
12	Authors' names,		
24	Paper title		

6.2. Text Layout for Accepted Papers

A4 page margins should be margins: top = 24 mm, bottom = 24 mm, side = 15 mm. The column width is 87mm (3.425 in). The space between the two columns is 6 mm (0.236 in). Paragraph indentation is 3.5 mm (0.137 in). Follow the type sizes specified in Table. Position figures and tables at the tops and bottoms of columns. Avoid placing them in the middle of columns. Large figures and tables may span across both columns. Figure captions should be centred below the figures; table captions should be centred above. Avoid placing figures and tables before their first mention in the text. Use the abbreviation "Fig. 1," even at the beginning of a sentence.

7. Submission Process

The International Journal of Engineering Technologies operates an online submission and peer review system that allows authors to submit articles online and track their progress via a web interface. Articles that are prepared referring to this template should be controlled according to submission checklist given in "Guide f Authors". Editor handles submitted articles to IJET primarily in order to control in terms of compatibility to aims and scope of Journal. Articles passed this control are checked for grammatical and template structures. If article passes this control too, then reviewers are assigned to article and Editor gives a reference number to paper. Authors registered to online submission system can track all these phases. Editor also informs authors about processes of submitted article by e-mail. Each author may also apply to Editor via online submission system to review papers related to their study areas. Peer review is a critical element of publication, and one of the major cornerstones of the scientific process. Peer Review serves two key functions:

- Acts as a filter: Ensures research is properly verified before being published
- Improves the quality of the research

8. Conclusion

The conclusion section should emphasize the main contribution of the article to literature. Authors may also explain why the work is important, what are the novelties or possible applications and extensions. Do not replicate the abstract or sentences given in main text as the conclusion.

Acknowledgements

Authors may acknowledge to any person, institution or department that supported to any part of study.

References

[7] J. Clerk Maxwell, A Treatise on Electricity and Magnetism, 3rd ed., vol. 2. Oxford:Clarendon Press, 1892, pp.68-73. (Book)

[8] H. Poor, An Introduction to Signal Detection and Estimation, New York: Springer-Verlag, 1985, ch. 4. (Book Chapter)

[9] Y. Yorozu, M. Hirano, K. Oka, and Y. Tagawa, “Electron spectroscopy studies on magneto-optical media and plastic substrate interface”, IEEE Transl. J. Magn. Japan, vol. 2, pp. 740-741, August 1987. (Article)

[10] E. Kabalcı, E. Irmak, I. Çolak, “Design of an AC-DC-AC converter for wind turbines”, International Journal of Energy Research, Wiley Interscience, DOI: 10.1002/er.1770, Vol. 36, No. 2, pp. 169-175. (Article)

[11] I. Çolak, E. Kabalci, R. Bayindir R., and S. Sagiroglu, “The design and analysis of a 5-level cascaded voltage source inverter with low THD”, 2nd PowerEng Conference, Lisbon, pp. 575-580, 18-20 March 2009. (Conference Paper)

[12] IEEE Standard 519-1992, Recommended practices and requirements for harmonic control in electrical power systems, The Institute of Electrical and Electronics Engineers, 1993. (Standards and Reports)

INTERNATIONAL JOURNAL OF ENGINEERING TECHNOLOGIES (IJET)
COPYRIGHT AND CONSENT FORM

This form is used for article accepted to be published by the IJET. Please read the form carefully and keep a copy for your files.

TITLE OF ARTICLE (hereinafter, "The Article"):

………..……………………………………………….....................………………………………………………………

………..……………………………………………….....................…………………………………………………………

…………..………………………………………………………………..……………………………………………

LIST OF AUTHORS:

………..…………………………………………………………..…..………………………………………………………

………..……………………………………………….....................…………………………………………………………

……………………………………………………………………..………………………………………..……………

CORRESPONDING AUTHOR'S ("The Author") NAME, ADDRESS, INSTITUTE AND EMAIL:

……………………………………………………………………..…………………………………………………………

………..……………………………………………….....................…………………………………………………………

…………..………………………………………………………………..…………………………………….……

COPYRIGHT TRANSFER

The undersigned hereby transfers the copyright of the submitted article to International Journal of Engineering Technologies (the "IJET"). The Author declares that the contribution and work is original, and he/she is authorized by all authors and/or grant-funding agency to sign the copyright form. Author hereby assigns all including but not limited to the rights to publish, distribute, reprints, translates, electronic and published derivates in various arrangements or any other versions in full or abridged forms to IJET. IJET holds the copyright of Article in its own name.

Author(s) retain all rights to use author copy in his/her educational activities, own websites, institutional and/or funder's web sites by providing full citation to final version published in IJET. The full citation is provided including Authors list, title of the article, volume and issue number, and page number or using a link to the article in IJET web site. Author(s) have the right to transmit, print and share the first submitted copies with colleagues. Author(s) can use the final published article for his/her own professional positions, career or qualifications by citing to the IJET publication.

Once the copyright form is signed, any changes about the author names or order of the authors listed above are not accepted by IJET.

Authorized/Corresponding Author **Date/ Signature**